



THE UNIVERSITY *of* EDINBURGH

Edinburgh Research Explorer

Was the cold European winter 2009-2010 modified by anthropogenic climate 1 change? An attribution study.

Citation for published version:

Tett, S 2018, 'Was the cold European winter 2009-2010 modified by anthropogenic climate 1 change? An attribution study.', *Journal of Climate*. <https://doi.org/10.1175/JCLI-D-17-0589.s1>.

Digital Object Identifier (DOI):

[10.1175/JCLI-D-17-0589.s1](https://doi.org/10.1175/JCLI-D-17-0589.s1).

Link:

[Link to publication record in Edinburgh Research Explorer](#)

Document Version:

Peer reviewed version

Published In:

Journal of Climate

General rights

Copyright for the publications made accessible via the Edinburgh Research Explorer is retained by the author(s) and / or other copyright owners and it is a condition of accessing these publications that users recognise and abide by the legal requirements associated with these rights.

Take down policy

The University of Edinburgh has made every reasonable effort to ensure that Edinburgh Research Explorer content complies with UK legislation. If you believe that the public display of this file breaches copyright please contact openaccess@ed.ac.uk providing details, and we will remove access to the work immediately and investigate your claim.



1 **Was the cold European winter 2009-2010 modified by anthropogenic climate**
2 **change? An attribution study.**

3 Bo Christiansen*

4 *Danish Meteorological Institute, Copenhagen, Denmark*

5 Carmen Alvarez-Castro

6 *Laboratoire des Sciences du Climat et de l'Environnement, Institut Pierre-Simon Laplace,*

7 *Université Paris-Saclay, Gif sur Yvette, France*

8 Nikolaos Christidis, Andrew Ciavarella

9 *UK Met Office Hadley Centre, FitzRoy Road, Exeter EX1 3PB, UK*

10 Ioana Colfescu

11 *National Centre for Atmospheric Science, University of Leeds, UK*

12 Tim Cowan

13 *School of GeoSciences, University of Edinburgh, Edinburgh EH9 3JW, UK*

14 Jonathan Eden

15 *Royal Netherlands Meteorological Institute (KNMI), De Bilt, Netherlands*

16 Mathias Hauser

17 *Institute for Atmospheric and Climate Science, ETH Zurich, Zurich, Switzerland*

18
19
20
21
22
23
24
25
26
27
28
29
30
31
32
33
34
35
36

Nils Hempelmann

*Laboratoire des Sciences du Climat et de l'Environnement, Institut Pierre-Simon Laplace,
Université Paris-Saclay, Gif sur Yvette, France*

Katharina Klehmet

Institute of Coastal Research, Helmholtz-Zentrum Geesthacht, Geesthacht, Germany

Fraser Lott

UK Met Office Hadley Centre, FitzRoy Road, Exeter EX1 3PB, UK

Cathy Nangini

*Laboratoire des Sciences du Climat et de l'Environnement, Institut Pierre-Simon Laplace,
Université Paris-Saclay, Gif sur Yvette, France*

Geert Jan van Oldenborgh

Royal Netherlands Meteorological Institute (KNMI), De Bilt, Netherlands

René Orth

Institute for Atmospheric and Climate Science, ETH Zurich, Zurich, Switzerland

Peter Stott

UK Met Office Hadley Centre, FitzRoy Road, Exeter EX1 3PB, UK

Simon Tett

School of GeoSciences, University of Edinburgh, Edinburgh EH9 3JW, UK

Robert Vautard

37 *Laboratoire des Sciences du Climat et de l'Environnement, Institut Pierre-Simon Laplace,*
38 *Université Paris-Saclay, Gif sur Yvette, France*

39 Laura Wilcox

40 *Department of Meteorology, University of Reading, P. O. Box 243, Earley Gate, Reading RG6*
41 *6BB, UK*

42 Pascal Yiou

43 *Laboratoire des Sciences du Climat et de l'Environnement, Institut Pierre-Simon Laplace,*
44 *Université Paris-Saclay, Gif sur Yvette, France*

45 **Corresponding author address: Bo Christiansen, Danish Meteorological Insti-*
46 *tute, Lyngbyvej 100, DK-2100 Copenhagen Ø, Denmark.*

47 E-mail: boc@dmi.dk

ABSTRACT

48 An attribution study has been performed to investigate the degree to which
49 the unusually cold European winter 2009-2010 was modified by anthro-
50 pogenic climate change. Two different methods have been included for the
51 attribution: one based on a large HadGEM3-A ensemble and one based on a
52 statistical surrogate method. Both methods are evaluated by comparing simu-
53 lated winter temperature means, trends, standard deviations, skewness, return
54 periods, and 5 % quantiles with observations. While the surrogate method
55 performs well, HadGEM3-A in general underestimates the trend in winter
56 by a factor of 2/3. It has a mean cold bias dominated by the mountainous
57 regions and also underestimates the cold 5 % quantile in many regions of Eu-
58 rope. Both methods show that the probability of experiencing a winter as cold
59 as 2009-2010 has been reduced by approximately a factor of two due to an-
60 thropogenic changes. The method based on HadGEM3-A ensembles gives
61 somewhat larger changes than the surrogate method because of differences
62 in the definition of the unperturbed climate. The results are based on two
63 diagnostics: the coldest day in winter and the largest continuous area with
64 temperatures colder than twice the local standard deviation. The results are
65 not sensitive to the choice of bias correction except in the mountainous re-
66 gions. Previous results regarding the behavior of the measures of the changed
67 probability have been extended. The counter-intuitive behavior for heavy-
68 tailed distributions is found to hold for a range of measures and for events that
69 become more rare in a changed climate.

70 **1. Introduction**

71 An increased frequency of occurrence of extreme events such as flooding and heat waves has
72 been reported (Frich et al. 2002; Alexander et al. 2006; Meehl et al. 2009; Coumou and Rahm-
73 storf 2012; Peterson et al. 2012; Fischer and Knutti 2015) and, as the potentially most adverse
74 consequences of climate change are related to extremes, there has been an increased interest in
75 the attribution of such events (see, e.g., Field et al. 2012; National Academies of Sciences, En-
76 gineering, and Medicine 2016). A particular challenge is the attribution of single events. While
77 there are a number of papers addressing event attribution of flooding and heat waves, there has
78 not been much work done in this area addressing cold spells. Cold spells also increase morbidity
79 and mortality, although the effect is weaker than for extreme warm events (Conlon et al. 2011).
80 Furthermore, extreme winter conditions have serious detrimental effects on infrastructure such
81 as damage to railways, closed airports, and frozen power lines (see, e.g., Doll et al. 2014, and
82 references therein).

83 Part of the lesser interest in the attribution cold spells – at least in Europe – can be found
84 in a weaker change in winter temperatures than in summer temperatures (see section 4). To-
85 gether with the larger natural variability in winter, this makes changes in cold spells harder to
86 detect. Cold spells in Europe are closely connected to the North Atlantic Oscillation (NAO) and
87 blocking (Buehler et al. 2011), with a negative NAO index suggestive of cold European winters.
88 Stratospheric sudden warmings propagate downwards on sub-seasonal time-scales and lead sta-
89 tistically to a negative phase of the NAO and associated colder temperatures in Europe (Baldwin
90 and Dunkerton 1999; Christiansen 2001). In addition to the general warming expecting to reduce
91 cold extremes (Van Oldenborgh et al. 2014), there have also been discussions about dynamical
92 effects related to anthropogenic forcings that may change European winter temperatures and cold

93 spells. One proposed connection is a positive correlation between autumn sea-ice extent and the
94 atmospheric circulation, e.g., the NAO, the following winter, which has been studied both in obser-
95 vations (Francis et al. 2009; Overland and Wang 2010; Liu et al. 2012; Tang et al. 2013) and with
96 modelling approaches (Petoukhov and Semenov 2010; Orsolini et al. 2011; Yang and Christensen
97 2012; Mori et al. 2014). In another model study Sévellec et al. (2017) found a link between sea-ice
98 and the Atlantic meridional overturning circulation. With retreating sea-ice due to a general warm-
99 ing – and the Arctic amplification of that warming – such connections could help to explain the
100 occurrence of recent cold winters in Europe. However, recent results (Li et al. 2015; Gerber et al.
101 2014; Screen 2017) suggest that the relationship between sea-ice, the NAO, and cold spells may
102 be a chance occurrence or at least is very fragile. Recently, Francis (2017) related the unsettled
103 science to a potential combination of a low signal-to-noise ratio and deficiencies in the models,
104 the experimental designs, and the metrics of circulation changes. Other broad review of the Arctic
105 influence on mid-latitudes are presented by Overland et al. (2015) and Cohen et al. (2014), while
106 the reviews by Vihma (2014) and Gao et al. (2014) focus on the connection between sea-ice and
107 mid-latitude weather and climate. Low-frequency changes in European cold spells may also be
108 related to an intensified anticyclone that drives changes in the Siberian high (Zhang et al. 2012).

109 Here, we present an event attribution study of the cold European winter 2009-2010. The at-
110 tribution is based on two different methods; the first is based on the ensembles produced by the
111 HadGEM3-A (Hadley Centre Global Environment Model version 3) atmospheric model and the
112 second on ensembles generated by a statistical surrogate method.

113 The paper is organized as follows. In section 2 we describe the data and the diagnostics used
114 for the event attribution of cold spells. Therein, we also briefly describe the meteorological details
115 of the winter 2009-2010 (see also WMO (2010)) focusing on these diagnostics. The two methods
116 for generating ensembles – the HadGEM3-A model and the statistical surrogate method – are de-

117 scribed in section 3. In section 4 we evaluate these two methods against observations. In section 5
118 we present the resulting risk ratios. In appendix A we expand the discussion of the framing issue
119 of attribution of single events from Christiansen (2015) to be more relevant for the present study.
120 The extension includes other measures of the risk than just the Fractional Attributable Risk and
121 also the situation where the considered event becomes less frequent in the changed climate. The
122 conclusions are presented in section 6.

123 **2. The observations, the diagnostics, and the winter 2009-2010**

124 For surface temperature observations we use the E-OBS (version 12) daily mean gridded data-set
125 on a 0.5x0.5 longitude/latitude land-only grid (Haylock et al. 2008). Uncertainties in the E-OBS
126 data and comparisons with re-analyses are presented in van der Schrier et al. (2013), who find
127 good agreement between European mean trends in the different data-sets.. We also use daily zonal
128 wind from the National Centers for Environmental Prediction/National Center for Atmospheric
129 Research reanalysis (NCEP/NCAR) reanalysis on a 2.5x2.5 longitude/latitude grid and 17 pres-
130 sure levels from 1000 to 10 hPa (Kalnay et al. 1996). To calculate the NAO index we use NCEP
131 daily sea-level pressure on a 2.5x2.5 longitude/latitude grid. For all three data sets we use the 54
132 year long period 1960-2013 which is also the period for which the experiments with HadGEM3-A
133 have been performed (see section 3). We select E-OBS data for Europe, defined here as latitudes
134 between 35 and 70° N and longitudes between 10° W and 30° E. For the E-OBS data we exclude
135 grid-points where more than 5 % of the days are missing data. This affects only small regions on
136 the African coast. Grid-points that are missing data between 0 and 5 % of the days are filled using
137 nearest neighbour interpolation. This affects a few grid-points on the African coast and in Turkey.

138 The NAO is calculated by empirical orthogonal function (EOF) analysis of winter (DJF) monthly
139 anomalies of sea-level pressure for latitudes between 20 and 80° N and longitudes between 90° W

140 and 40 ° E. The anomalies are first weighted by the square-root of the cosine of the latitudes and
141 linearly detrended. Daily values of the NAO index are then found by projecting the leading EOF
142 onto daily sea-level pressure anomalies (see, e.g., Blessing et al. 2005).

143 There are many possible diagnostics of the severity of cold winters including different combi-
144 nations of the duration, extent, and intensity of the cold periods. In the following we focus on two
145 diagnostics. The first diagnostic is defined on grid-cell scales as the minimum temperature over
146 the whole winter. The second diagnostic, herefrom denoted the blob index, is a spatially integrated
147 measure defined as the largest continuous area with temperature anomalies less than -2σ , where
148 σ is the local, seasonally varying standard deviation, i.e., the standard deviation calculated for
149 each grid-point and for each day of the year. Thus, the blob index is a combined measure of both
150 the spatial coherence and the intensity of the cold spell. The blob index is calculated for each day
151 separately and for convenience expressed as a fraction of the total European land area. Both diag-
152 nostics are calculated from daily mean temperatures. The first diagnostic measures the intensity
153 of the cold period while the second diagnostic also takes spatial extent into account, and is similar
154 to the heat-wave diagnostic used in Christiansen (2015).

155 We now briefly describe the winter 2009-2010 with focus on the chosen diagnostics; the mini-
156 mum temperature over whole winter and the blob index. The winter 2009-2010 was a relatively
157 cold winter with a series of strong cold spells of which the strongest appeared in the middle of
158 December. The blob index reached a value of 0.38 on 19th December (Fig. 1, top panel), which
159 is large but exceeded in both earlier and later winters, e.g., in the winter of 2011-2012. On 19th
160 December 2009 the temperature was below normal almost everywhere except for few regions in

161 Northern Scandinavia (Fig. 2). The coldest anomalies, below -4σ , are found in the middle of
162 Germany¹.

163 The temperature of the coldest day of the winter 2009-2010 confirms that this year was unusually
164 cold in many regions of Europe (Fig. 3). In Germany, Spain, Great Britain, and Scandinavia
165 temperatures as cold as in 2009-2010 are rarely found in other years in the period 1960-2013.

166 The winter 2009-2010 was, as many other cold winters, dominated by a strong negative NAO
167 (Wang et al. 2010; Ouzeau et al. 2011; Buchan et al. 2014) (demonstrated in the upper panel
168 of Fig. S1 in the supplement). However, this winter might not have been as cold as previous
169 winters with the same NAO levels, suggesting an impact of a general warming climate (Cattiaux
170 et al. 2010). The negative NAO was connected to a weak stratospheric vortex (Cohen et al. 2010;
171 Vargin 2015) – as demonstrated in the lower panel in Fig. S1 – although the main factor responsible
172 for the strong negative NAO has been suggested to be related to internal tropospheric dynamical
173 processes (Jung et al. 2011).

174 **3. The two ensemble methods**

175 To make statements about the attributable risk of the observed extreme event (the winter 2009-
176 2010) we need information about the frequencies of similar events of different magnitudes in both
177 the unperturbed climate and in the climate under anthropogenic forcings (Allen 2003; Stott et al.
178 2004, 2013). For each of the climates the probability for finding an event at least as extreme
179 as the observed event is calculated. The risk ratio is then defined as the ratio between these
180 two probabilities. See also appendix A for a more precise definition of the risk ratio and other
181 measures of the attributable risk. To obtain these frequencies we here use ensembles both from

¹The lead author got stuck in airports in Manchester and then Amsterdam on the way home from AGU. The meteorological conditions are described here https://en.wikipedia.org/wiki/Winter_of_2009-2010_in_Europe

182 the atmospheric general circulation model HadGEM3-A and ensembles obtained by a surrogate
183 field method that produces fields with the same spatial and temporal structure as an observed target
184 field. These methods complement each other as they make different assumptions about the effect of
185 anthropogenic climate change. Note, that for the HadGEM3-A approach the unperturbed climate
186 is represented by pre-industrial (1850) conditions while for the surrogate method it is represented
187 by 1960 conditions.

188 *a. The dynamical model*

189 Two ensembles, each with 15 members, have been produced with HadGEM3-A covering the
190 years 1960-2013. The horizontal resolution is N216 and the vertical resolution is L85 with 50
191 tropospheric and 35 stratospheric layers. The version used here is discussed in Ciavarella et al.
192 (2017) and includes the Global Atmosphere 6.0 (GA6) atmospheric science package (Walters et al.
193 2016). Both ensembles were recently used for attribution analysis by Christidis et al. (2016), Eden
194 et al. (2016), and Burke et al. (2016). A detailed analysis of the perturbed (historical) ensemble
195 regarding the skill in extreme events is presented in Vautard et al. (2017). We further note that no
196 significant correlations between the Arctic autumn sea-ice and the winter NAO are found in these
197 ensembles. This holds both when total Arctic sea ice and regional sea-ice (e.g., the Kara-Barents
198 Seas) is considered.

199 The two ensembles differ through the external climate forcings included, one is driven with both
200 natural and anthropogenic forcings (historical) and the other with only natural forcings (histnat).
201 Natural external forcings are variability in total solar irradiance at the top of the atmosphere, and
202 volcanic activity implemented through a latitudinal variation of stratospheric aerosol optical depth.
203 Anthropogenic forcings include well-mixed greenhouse gases, zonal-mean ozone concentrations,
204 aerosol emissions, and land use changes. The external forcings are obtained from sources used by

205 the Coupled Model Intercomparison Project Phase 5 (CMIP5) generation of models (Taylor et al.
206 2011). In the histnat experiments, anthropogenic forcings are held at pre-industrial levels taken to
207 be those of 1850. Boundary conditions at the bottom of the atmosphere are given by sea-surface
208 temperatures (SST) and sea-ice concentrations fields. In the historical experiments the SSTs and
209 the sea-ice are prescribed from observed values (HadISST1.1, Rayner et al. 2003) while for the
210 histnat experiments an estimate of the change due to anthropogenic influence is removed from the
211 observations (Christidis et al. 2013). This estimate comes from ensembles of simulations with and
212 without anthropogenic forcings generated with 19 coupled models for the C20C+ detection and
213 attribution project (<http://portal.nerisc.gov/c20c/experiment.html>).

214 Both ensembles share a common atmospheric initialization on 1st December 1959 from ERA-40
215 reanalysis fields (Uppala et al. 2005). The differences between ensemble members are produced
216 by two stochastic physics schemes that generate small differences in the physics of each simula-
217 tion (Christidis et al. 2013).

218 *b. Ensemble surrogate field method*

219 The method is based on a simple algorithm to produce ensembles of surrogate fields based on
220 observations. This method produces surrogate fields with the same spatial and temporal structure
221 – as measured with instantaneous and lagged cross-correlations – as the original observed field of
222 surface temperatures. The method was used in Christiansen (2015) for attribution of heat waves
223 and in a study of the significance of the increase in warm records (Christiansen 2013). The sur-
224rogate fields are generated with a phase-scrambling procedure described in Christiansen (2007,
225 2013) which is very similar to the multivariate method introduced by Prichard and Theiler (1994)
226 based on the univariate amplitude adjusted Fourier transform method (AAFT) by Theiler et al.
227 (1992).

228 The general outline of the procedure is familiar from bootstrap methods; first a transformation
229 of the original field into stationary anomalies is performed, stationary surrogate anomalies are pro-
230 duced from the original stationary anomalies, and the final surrogate field is produced by applying
231 the inverse transformation to the surrogate anomalies.

232 The stationary anomalies of the original observed surface temperature field are obtained by
233 removing the average annual cycle and the secular variations – trends and variability on the lowest
234 frequencies estimated by a 3rd order polynomial fit – at each geographical position. The resulting
235 stationary anomalies are Fourier transformed, then the Fourier phases are randomized but with
236 the same random phases for all grid-points, and finally inverse Fourier transforms are performed
237 to get the stationary surrogate anomalies. Now the average annual cycles are restored at each
238 geographical position to get a surrogate field of the unperturbed climate state, i.e., ‘the world that
239 could have been without climate change’. Also adding the secular trends to this field gives us a
240 surrogate of the perturbed climate.

241 Repeating this process with different randomizations allows us to calculate ensembles of fields
242 for both the unperturbed climate and the perturbed climate. From these ensembles the relevant
243 distributions of the diagnostic can be calculated and the risk ratio for an observed event can be
244 estimated.

245 The surrogate method is fast and flexible and can therefore also be used for sensitivity studies
246 and to test the robustness of the risk ratio to methodological choices. The method does not depend
247 on physical parameterizations but only on statistical assumptions. A fundamental assumption
248 is that it is possible in the observations to empirically separate internal variability from climate
249 change. Here this separation is performed by assuming different temporal scales for the two types
250 of variability. The method was tested in details in Christiansen (2015) and found to be adequate
251 for temperature fields while problems may arise for fields which are strongly non-Gaussian. In

252 agreement with the analysis in Christiansen (2015) we find here similar results for cold spells
253 when climate change is defined by 5th or 7th order polynomials.

254 **4. Evaluation**

255 In this section we investigate the extent to which HadGEM3-A and the surrogate methods repro-
256 duce the relevant features of the observations. Our confidence in the calculated risk ratios depends
257 on the methods ability to reproduce long-term temperature trends as well as cold extremes.

258 The statistical significance of trends and differences is estimated by Monte-Carlo methods that
259 take the possible serial correlations of the data into account. The statistical significance of trends
260 are calculated by a phase-scrambling method (Theiler et al. 1992; Christiansen 2001) for which
261 the ‘bootstrap’ members retain the full auto-correlation spectrum of the original detrended time-
262 series. The significance of differences are calculated by a block-bootstrap method assuming that
263 data separated by 15 days are independent. This separation corresponds to roughly twice the
264 temporal decorrelation length of surface temperatures (see, e.g., Christiansen 2015).

265 We will use ‘historical’ and ‘histnat’ to denote the two ensembles from HadGEM3-A. For the
266 surrogate method we use ‘perturbed’ and ‘unperturbed’ ensembles. So ‘histnat’ and ‘unperturbed’
267 ensembles refer to the counter-factual world that could have been.

268 Some general evaluations related to cold spells were presented in Vautard et al. (2017) based
269 on the historical HadGEM3-A ensemble. It was concluded that there were no major processes
270 hindering the representation of cold spells. Here we will focus on quantities directly related to the
271 two diagnostics and compare the evaluations of the dynamical model and the surrogate method.

272 *a. The European mean perspective*

273 The observed spatially averaged European winter (DJF) mean temperature has a linear trend
274 of 0.30 °C/decade (95 % confidence interval is [0.12, 0.51] °C/decade) in the period 1960-2013
275 (Fig. 4). This is somewhat larger than the ensemble mean of the HadGEM3-A historical ensemble
276 which shows a trend of 0.20 °C/decade (95 % interval [0.12, 0.28]). Both these trends are sig-
277 nificant to the 5 % level while only approximately half of the individual HadGEM3-A historical
278 ensemble members show significant trends. However, 3 out of the 15 ensemble members show a
279 trend that is comparable to that of the observations. The trends are probably due to a combina-
280 tion of increasing greenhouse gases and decreasing European aerosol emissions. However, there
281 is no significant difference in the trends calculated for the whole period, the period before 1985,
282 and the period after 1985, neither for observations nor models. It is also worth noting that the
283 HadGEM3-A model has a negative bias which is dominated by mountainous regions as seen in
284 the next sub-section.

285 The ensemble mean of the perturbed ensemble of surrogates has a linear trend of 0.34 °C/decade
286 (significant to the 5 % level, 95 % interval [0.26, 0.42]) close to that of the observations as should
287 be expected by construction. The ensemble of surrogates shows less variation among ensemble
288 members than does the HadGEM3-A ensemble, and all of them show significant trends. The
289 unperturbed ensemble mean and the histnat ensemble mean show weak and insignificant trends.
290 The NAO index has a weak non-significant trend in the observations while it is almost zero in the
291 two HadGEM3-A ensembles (not shown).

292 The correlation of the European mean winter temperature between observations and the ensem-
293 ble mean of the HadGEM3-A historical ensemble is 0.47 (95 % confidence interval is [0.15, 0.71]).
294 For the HadGEM3-A histnat ensemble the correlation is 0.29 ([0.01, 0.53]). As expected the cor-

relations for the surrogate ensembles are smaller, 0.28 ($[-0.14, 0.60]$) and 0.02 ($[-0.28, 0.32]$), reflecting that for this method only the trend will contribute. For the observations the correlation between the European mean winter temperature and the NAO index is 0.67 ($[0.40, 0.82]$), and similar values (0.61 and 0.63) are found for the two HadGEM3-A ensembles. Correlations of winter mean NAO index between observations and the two HadGEM3-A ensemble means are 0.19 ($[-0.03, 0.41]$) and 0.22 ($[-0.03, 0.46]$), while the correlation between the NAO index in the two ensemble means is 0.52 ($[0.29, 0.70]$). Thus, for both observations and the HadGEM3-A ensembles the SSTs determine a considerable part of the average European land temperature and the NAO index and the land temperature are well correlated. However, the NAO itself is only to a limited extent determined by SSTs (see, e.g., Greatbatch 2000, and references therein).

To get an overall impression of the changes in winter extremes we normalize the local temperatures for each grid-point with the local, seasonally varying standard deviation (calculated for each grid-point and for each day of the year) and pool them all together (Fig. 5). The challenge of detection and attribution of cold extremes becomes clear: although there is a general change in the distributions the changes are particularly small for the cold tail. This is quantitatively different from summer temperatures (Fig. S2) which show a general shift of the whole distribution toward warmer values. Both the HadGEM3-A historical ensemble and the perturbed surrogate show changes comparable to observations. Note also that the distributions in winter are heavily negatively skewed so that the values in the negative tail are numerically larger than those in the positive tail. This is in agreement with the observation (Twardosz and Kossowska-Cezak 2016) that more extreme cold than extreme warm winters are observed.

The blob diagnostic combines intensity and spatial coherence of the cold spell and requires a specific validation. In Fig. 1 the diagnostic is shown as function of time for a random historical HadGEM3-A ensemble member and for a random perturbed surrogate ensemble member. The two

319 ensemble members compare well with observations. Figure 6 shows the return periods including
320 only winter days of the historical HadGEM3-A and the perturbed surrogate ensembles, as well as
321 for observations. We see that both the surrogate method and HadGEM3-A reproduce the observed
322 return periods of the largest continuous area very well. However, there is a tendency for the
323 HadGEM3-A to overestimate the return periods for events smaller than 0.35.

324 *b. The local perspective*

325 In sub-section 1 we present an evaluation based on all winter days while we in sub-section 2
326 briefly add to the evaluation of the temperatures of the coldest winter days presented in Vautard
327 et al. (2017).

328 1) EVALUATION BASED ON ALL WINTER DAYS

329 The mean of the local temperatures over the winters 1960-2013 is relatively well modelled
330 in the historical HadGEM3-A ensemble (Fig. 7), with a bias that is small (although statistically
331 significant) except for the alpine region and regions in Northern Scandinavia. In these mountainous
332 regions the model is up to 5°C colder than the observations. The long term mean difference
333 between the historical and histnat model is statistically significant and positive everywhere with
334 the strongest warming in the north eastern part of Europe – reaching 4°C in Finland – and the
335 weakest warming in the south western part. For the surrogate method (not shown) the long term
336 mean is by construction almost indistinguishable from that of the observations.

337 The linear trend of the local temperatures over the winters 1960-2013 (Fig. 8) is positive nearly
338 everywhere in the observations with the largest trends in the north eastern regions. The trends
339 are statistically significant in large areas. The same pattern but of weaker strength and lower
340 significance is found in the historical HadGEM3-A experiments (see also Vautard et al. (2017)).

341 The trends for the perturbed surrogate have the same magnitude as in observations. For the histnat
342 and unperturbed ensembles the trends are close to zero everywhere. The pattern of the differences
343 in the mean between HadGEM3-A historical and histnat ensembles (bottom right panel in Fig. 7)
344 and the trends in observations and the HadGEM3-A historical ensembles (left panels in Fig. 8) are
345 in general agreement with the expected Arctic amplification.

346 The standard deviation, the skewness, and the 5 % quantile of the local temperatures are shown
347 in Figs. 9, 10, and 11. These quantities are calculated from winter anomalies over the period 1960-
348 2013 after removing the seasonal cycle and the secular trend in form of a 3rd order polynomial
349 fit. The figures include the observations (upper panels), the historical HadGEM3-A and perturbed
350 surrogate (middle panels), the difference between the historical HadGEM3-A and observations
351 and the difference between the historical and histnat HadGEM3-A (lower panels).

352 Compared to the observations, the standard deviation in the historical HadGEM3-A model is
353 overestimated in the mountainous regions (Fig. 9). The modelled skewness is strongly overesti-
354 mated compared to observations in Scandinavia, while it is underestimated in north-eastern parts
355 of Europe. Only small differences are found in southern Europe (Fig. 10). The 5 % quantile is
356 overestimated in the model compared to observations in parts of Northern Europe while it is un-
357 derestimated in the mountainous regions (Fig. 11). This is a combination of the differences in
358 standard deviation and skewness.

359 Comparing the HadGEM3-A historical and histnat experiments we find smaller differences. The
360 standard deviation in the historical version is larger everywhere compared to the histnat version but
361 the differences are small. The 5 % quantile has increased everywhere except for Spain, although
362 the differences are statistically significant only in few regions. The pattern of the changes in the 5
363 % quantile is largely in agreement with the patterns of the changes in the long term means and the
364 trends in the historical HadGEM3-A model.

365 The comparison above was done with a single ensemble member. But the described results are
366 robust across the ensemble members and similar results are found for the ensemble mean. For the
367 perturbed surrogate the long term values of standard deviations, skewness, and 5 % quantile are
368 very well represented as expected.

369 For a good representation of the extremes it is not only necessary that the long term values of
370 the variance and skewness are well represented; also the year-to-year variations of these quantities
371 should be correctly represented. The spatial averages of the winter means of temperature, the
372 variance, and the skewness are shown as a function of the year in Fig. 12 for observations, for a
373 historical HadGEM3-A ensemble member, and for a perturbed surrogate. It is obvious that the
374 observed temporal variability of these quantities are well represented by both the HadGEM3-A
375 and the surrogate. The main deviation is the cold bias in the HadGEM3-A mentioned earlier. The
376 anti-correlation between winter means and variances was also observed in (Yiou et al. 2009).

377 2) EVALUATION OF THE COLDEST WINTER DAYS

378 Fitting a generalized extreme value (GEV) distribution to the coldest winter days Vautard et al.
379 (2017) found that the historical HadGEM3-A experiments underestimate the location parameter in
380 the mountainous regions. This is in agreement with the results for the 5 % quantile presented in the
381 previous sub-section. The scale parameter is reasonably well represented but in Eastern Europe
382 the model overestimates the shape parameter (too long cold tail). Again, this is in agreement with
383 the results for the skewness shown in the previous sub-section.

384 Here we use a Kolmogorov-Smirnov test to see if observed and modelled distributions of the
385 temperatures of the coldest winter days are equal. We also show how different forms of bias
386 correction change the results of the test. This is important when choosing the form of correction
387 used when calculating the risk ratios (section 5). The test is applied to each grid-point and for

388 each grid-point the observed sample consists of 53 numbers (one value for each winter) and the
389 modelled sample of 53*15 numbers (as we have 15 ensemble members). As a measure of the
390 overall similarity of the observed and modelled coldest days we use the fraction of grid-points for
391 which we can reject the null-hypothesis of identical distributions at the 5 % level.

392 For the raw data from the HadGEM3-A historical experiments we can reject the null-hypothesis
393 at the 5 % level in 71 % of the grid-points. The p-values from the test are shown in Fig. S3. For the
394 perturbed surrogate ensembles the corresponding fraction is only 7.5 %, indicating that the cold
395 extremes are well represented by the surrogate approach.

396 If we perform a bias correction with the difference between the means over all winter days (not
397 just the coldest) a small improvement is seen; now the null-hypothesis is rejected for a smaller
398 fraction, 61 %, of the grid-points. If we also scale with the standard deviations of all winter days
399 (so the observations and model both have same mean and same variance in each grid-point) we
400 get a drastic improvement to 26 %. However, bias correction with the mean of only the coldest
401 winter days brings the fraction of grid-points where we can reject the null-hypothesis down to 5.4
402 %. Thus some differences in the distributions are particular to the extremes; the differences can
403 not just be described as differences in the mean and standard deviations of winter days.

404 Fortunately, although the different corrections have different – and in some cases substantial
405 – influence on the distributions themselves we find that for the risk ratios the influence of the
406 corrections are rather small (section 5).

407 **5. The risk ratios**

408 The distributions of the temperatures of the coldest winter days and of the blob index have
409 been calculated for both the HadGEM3-A ensembles (historical and histnat) and the surrogate
410 ensembles (perturbed and unperturbed).

411 The significance and error bars have been calculated by bootstrapping the values contributing to
412 each distribution. For temperature of the coldest day this amounts to 15×53 values: one value for
413 each winter in each of the 15 ensembles. For the blob index it is $15 \times 53 \times 90$ values as we have 90
414 values each winter. Note that the resulting significance and error bars only include the effects of
415 finite ensemble size.

416 For the temperatures of the coldest winter days the distributions are calculated for each grid-
417 point. Two examples are shown in Fig. 13; a grid-point near Oslo and a grid-point near Utrecht.
418 These grid-points are typical for mountainous and non-mountainous regions, respectively. Consid-
419 ering first HadGEM3-A, we see that for both locations the distributions for the historical ensemble
420 have moved towards warmer values compared with the histnat ensemble. For the grid-point near
421 Utrecht the modeled distribution and the observations (grey vertical lines) agree well. For this
422 location the risk ratio of the winter 2009-2010 is 0.44 but it should be noted this winter was not
423 extreme at this location. Recall that a risk ratio less than one indicates a reduced probability for
424 an event as extreme as the observed. For the grid-point near Oslo the modeled distribution and the
425 observations do not agree (see discussion of model bias in section 4). The observed winter 2009-
426 2010 (vertical green line) is a cold winter at this location but falls in the middle of the modelled
427 distributions. Correcting the observed temperature for the mean winter bias (orange vertical line)
428 improves the situation significantly. Without the bias correction the risk ratio is 0.44 and with the
429 bias correction it is 0.05. Norway is the region where the bias correction has the largest impact
430 followed by the Alpine region. Outside these areas the effect of the bias correction on the risk
431 ratio is typically less than 0.15. Considering the surrogate method we find as expected that the
432 changes in the modelled distributions are smaller and that the distributions compare well with the
433 observations. Now the risk ratios are 0.71 for both locations.

434 The geographical distribution of the risk ratios for the coldest winter day is shown in Fig. 14.
435 We see that the probability for a 2009-2010 event has been reduced over almost all of Europe.
436 This holds for both the HadGEM3-A based analysis and the surrogate method although most val-
437 ues are moderate. The HadGEM3-A based analysis in general gives larger changes (and more
438 significant grid-points) than the surrogate method which can be understood from the fact that the
439 histnat ensemble with HadGEM3-A represents pre-industrial conditions while the corresponding
440 unperturbed ensemble with the surrogate method represents the 1960s. The mean risk ratio over
441 Europe is 0.69 for HadGEM3-A. Although, as we saw in section 2, bias correction will influence
442 the distributions themselves it has a smaller effect on the risk ratios outside the mountainous re-
443 gions. Correcting with the mean of all winter days gives a mean risk ratio of 0.65, while correcting
444 with the mean of the coldest days gives a mean risk ratio of 0.69.

445 Using only data since 1985 (bottom panel of Fig. 14) we find lower risk ratios for both the
446 HadGEM3-A and the surrogate methods. This should be expected as this period is warmer than
447 the period 1960-1985 in the histnat and perturbed ensembles. However, the lower risk ratios may
448 also partly be due to the smaller number of degrees of freedom in the shorter period (see Appendix
449 A).

450 The risk ratio of the 2009-2010 event measured with the blob index – which combines the
451 spatial coherence and the intensity of the cold spell – is shown Fig. 15. When the whole period is
452 considered the risk ratio of the 2009-2010 event is not significantly different for either HadGEM3-
453 A or the surrogate method. However, when only data from 1985 are considered the risk ratio
454 is 0.47 (95 % confidence interval is [0.36,0.58]) for HadGEM3-A and 0.65 ([0.50,0.82]) for the
455 surrogate method, and is significantly different from 1 in both cases. Again HadGEM3-A gives
456 larger and more significant changes than the surrogate method. Note that for the largest values of
457 the blob index the 95 % confidence intervals are based on few events and are therefore not robust.

458 Although the result that risk ratios differ more from 1 when calculated from the period after 1985
459 than when calculated from the whole period is in agreement with a stronger warming there might
460 also be an effect of the selection problem. In the longer period there is more events to choose from
461 (i.e., it includes more independent degrees of freedom) and the longer period will therefore favor
462 risk ratios closer to 1 (see section 6 and the analytic explanation in appendix A).

463 **6. Conclusions**

464 We have investigated the possibility of attributing the cold European winter 2009-2010 to anthro-
465 pogenic changes. Two different methods for event attribution have been included: one based on
466 the HadGEM3-A ensembles and one based on the statistical surrogate method described in Chris-
467 tiansen (2015). The surrogate method is based on a simple algorithm to produce ensembles of
468 surrogate fields for both the unperturbed climate and the perturbed climate. These ensembles
469 differ locally by the observed secular low-frequency variability. The method is based on observa-
470 tions and the surrogate fields by construction have the same spatial and temporal structure as the
471 original observed field. The HadGEM3-A ensembles differ in applied forcings, with the histnat
472 ensemble including only natural forcings and the historical ensemble also including the effects of
473 anthropogenic changes. While the histnat HadGEM3-A ensemble represents pre-industrial (1850)
474 conditions the unperturbed surrogate ensemble represents 1960 conditions.

475 Focusing the evaluation on HadGEM3-A, we found that the trend in winter means over 1960-
476 2013 is in general under-estimated by a factor of 2/3 although there is a considerable spread among
477 the ensemble members. HadGEM3-A also has a mean cold bias dominated by the mountainous
478 regions. The modelled winter standard deviation compares well to observations except for the
479 Norwegian coast and the Alpine region where it is somewhat overestimated. In observations the
480 skewness is negative almost everywhere. The model underestimates the strength of the nega-

481 tive skewness in Scandinavia and many of the western parts of Europe while it overestimates the
482 strength of the negative skewness in central Europe. Together this results in the cold 5 % quantile
483 being overestimated in many regions of Europe except in the mountainous areas. For the extremes
484 – such as the coldest day in winter – we do find some differences between the HadGEM3-A en-
485 semble and the observations. Fortunately, the risk ratios are not sensitive to these deficiencies.

486 For the attribution we considered two diagnostics; the coldest day in winter for each grid-point
487 and the largest continuous area with temperatures more than two local standard deviations below
488 the mean. The results for the risk ratio were presented using both the whole period 1960-2013 and
489 the later period 1985-2013 to build the distributions. For the largest continuous area no significant
490 change in the risk ratio was found for either the HadGEM3-A model or the surrogate method
491 when the whole period was included. When only the briefer period was included both methods
492 gave statistically significant (different from 1 at the 5 % level) risk ratios for the 2009-2010 event
493 of around 0.5. For the temperature of the coldest day in winter, values less than 1 were found over
494 most of Europe. Lower values were found for HadGEM3-A compared to the surrogate method.
495 Smaller and more significant values were found when only the later period was considered. For
496 this period the HadGEM3-A model and the surrogate method agree on the general pattern with the
497 lowest values in the Western Europe (except the Norwegian coast).

498 In the perturbed surrogates any low-frequency effect of retreating sea-ice would automatically be
499 included while, as mentioned in section 3a, there are no significant correlations between the Arctic
500 autumn sea-ice and the winter NAO in the HadGEM3-A historical ensemble. The latter observa-
501 tion does not completely rule out an influence of sea-ice on the temperatures in the HadGEM3-A
502 ensemble. However, the fact that we get comparable results about the risk ratios in both the sur-
503 surrogate method and the HadGEM3-A approach suggests that the effect of retreating sea-ice is not
504 very important for the risk ratios.

505 In appendix A we addressed some issues of attribution of single events. We saw that the counter-
506 intuitive behavior found for the Fractional Attributable Risk (FAR) in Christiansen (2015) also
507 holds for the risk ratio and the simple ratio of probabilities; these measures do not increase mono-
508 tonically with the strength of the event for heavy tailed distributions. As shown in Vautard et al.
509 (2017) cold extremes might actually have distributions that are difficult to distinguish from heavy
510 tailed distributions (shape parameters of GEV distributions close to 0). Note also that the risk
511 ratios found with the surrogate approach (Fig. 15) do not show a clear decrease with the strength
512 of the event. We also saw that all three measures are sensitive to the ‘selection problem’; they
513 depend on the number of degrees of freedom and therefore on the choice of region and period
514 used when counting the events that are similar to the observed extreme event. In agreement with
515 the analytical results we found in section 5 that the risk ratios for the whole period were larger
516 than the risk ratios for the period after 1985. Although some of the explanation can be found in the
517 increased warming in the later period, it further demonstrates that the attribution of single events
518 contains some amount of subjectivity. This point is emphasized by the very low risk ratios found
519 when only the period 2007-2012 is considered (bottom row in Fig. 15). In fact, even lower risk
520 ratios are found when only the winter 2009-2010 is considered (not shown). Finally we saw that
521 the issues described in Christiansen (2015) also exist when the event under consideration becomes
522 less frequent in the changed climate as for the cold events of the present study.

523 However, we take some comfort in the fact that the two very different methods in general agree
524 on the risk ratio. As mentioned above, the somewhat larger changes found for HadGEM3-A com-
525 pared to the surrogate approach are because the histnat and the unperturbed ensembles represent
526 different periods. As mentioned in Christiansen (2015) the surrogate method has both advantages
527 and disadvantages, the main advantages being that it is fast and does not require extensive com-
528 puter resources. The results in the present paper confirm that the surrogate method can be used as

529 an alternative for dynamical methods when considering event attribution. It is also reassuring that
530 the two very different diagnostics in general agree on a reduced risk of cold spells.

531 *Acknowledgments.* This work was supported by the EUCLEIA project funded by the European
532 Union's Seventh Framework Programme [FP7/2007-2013] under Grant Agreement No. 607085.
533 The NCEP Reanalysis data were provided by the NOAA-CIRES Climate Diagnostics Center,
534 Boulder, Colorado, USA, from their Web site at <http://www.cdc.noaa.gov/>. We acknowledge the
535 E-OBS dataset from the EU-FP6 project ENSEMBLES (<http://ensembles-eu.metoffice.com>) and
536 the data providers in the ECA&D project (<http://www.ecad.eu>). P. Yiou and C. Alvarez-Castro
537 were supported by ERC Grant No. 338965-A2C2.

538 APPENDIX

539 **Framing issues in attribution of single events**

540 There is an ongoing debate about the interpretation and usefulness of the attribution of single
541 events to climate change (Bindoff et al. 2013; Hansen et al. 2014; Hannart et al. 2015; Otto et al.
542 2015; Christiansen 2015; National Academies of Sciences, Engineering, and Medicine 2016). In
543 particular, Christiansen (2015) studied the influence of heavy tails and the 'selection problem', i.e.,
544 the consequence of the fact that the event under consideration is not independent but selected pre-
545 cisely because it is an extreme. While Christiansen (2015) focused on the Fractional Attributable
546 Risk we here expand the study to include other measures. We will also include the situation where
547 the event under consideration becomes more rare in the changed climate (as expected for cold
548 spells).

549 The situation and notation are briefly described as follows. For an observation x we denote the
550 probability density in the unperturbed climate as $p^{uc}(x)$ and the cumulative density as $P^{uc}(x)$. In

551 the perturbed climate the corresponding quantities are $p^{pc}(x)$ and $P^{pc}(x)$. Here, the perturbed
552 climate refers to the climate under anthropogenic changes and the unperturbed climate to ‘the
553 world that might have been’, i.e., the climate without anthropogenic changes. An often used
554 measure of the increased risk for x is the Fractional Attributable Risk (FAR) defined as $(\tilde{P}^{pc}(x) -$
555 $\tilde{P}^{uc}(x))/\tilde{P}^{pc}(x)$, where $\tilde{P} = 1 - P$ (Allen 2003; Stott et al. 2004, 2013). Here, we assume an event
556 on the right tail of the distribution. Other possible measures are the risk ratio $\tilde{P}^{pc}(x)/\tilde{P}^{uc}(x)$ and
557 the simple ratio of probabilities $p^{pc}(x)/p^{uc}(x)$.

558 We first assume that climate change amounts to a simple shift $p^{pc}(x) = p^{uc}(x - c)$, $c = 0.3$. This
559 is a reasonable first order approximation as discussed in Christiansen (2015). Also note that in a
560 study of climate-model simulations with future levels of greenhouse gases, de Vries et al. (2012)
561 finds that changes in the frequency of cold spells in Western Europe can be explained by changes
562 in the mean and variance. Under this assumption, Christiansen (2015) showed that while the FAR
563 increases monotonically with x when $p^{uc}(x)$ is Gaussian, this is not the case when $p^{uc}(x)$ has a
564 heavy tail. In this case the FAR has a maximum for a finite value of x . Christiansen (2015) also
565 studied the effect of the ‘selection problem’ defined above. In this case the relevant probability is
566 not $p^{uc}(x)$ but rather $p_n^{uc}(x_{max})$: the probability density of the largest value, x_{max} , of n variables.
567 Note, that when the n variables are independent and identically distributed we have the identity
568 $P_n = P^n$ for the cumulative densities.

569 While Christiansen (2015) only considered the FAR, we here show results also for the risk ratio
570 and the simple ratio $p^{pc}(x)/p^{uc}(x)$ (Fig. A1). We see that all three measures behave similarly.
571 Under Gaussianity (left panels) they all increase with x and approach infinity for large x . However,
572 for the distribution with the heavy tail (right panels), they all have a maximum whereafter they
573 decrease. Also note, that for a given x all measures decrease as the number of degrees of freedom
574 increases.

575 The analysis above assumes that the event under consideration becomes more frequent in the
576 changed climate. For the cold spells analysed in the present paper – and a few previous attribution
577 studies (Christidis et al. 2013, 2014) – the situation is the opposite. The relevant assumption is
578 now $p^{pc}(x) = p^{uc}(x + c)$. Results for this case is shown in Fig. A2. Now the FAR and the two
579 other measures decrease monotonically under Gaussianity while for distributions with heavy tails
580 they reach a minimum for a finite value of x . We also see that all measures increase as the number
581 of degrees of freedom increases.

582 Thus, the conclusions of Christiansen (2015) based on the FAR also hold for the other measures
583 and when the considered event becomes more infrequent. The ‘selection problem’ cannot be
584 avoided; all three measures change drastically when the number of degrees of freedom increases.
585 All three measures are sensitive to deviations from Gaussianity; for heavy-tailed distributions the
586 measures do not change monotonically so for the most extreme events the measures reports less
587 changes in the risk than for more intermediate values.

588 **References**

589 Alexander, L. V., and Coauthors, 2006: Global observed changes in daily climate extremes of
590 temperature and precipitation. *J. Geophys. Res.*, **111**, D05 109, doi:10.1029/2005JD006290.

591 Allen, M., 2003: Liability for climate change. *Nature*, **421 (6926)**, 891–892.

592 Baldwin, M. P., and T. J. Dunkerton, 1999: Propagation of the Arctic Oscillation from the strato-
593 sphere to the troposphere. *J. Geophys. Res.*, **104**, 30 937–30 946.

594 Bindoff, N. L., and Coauthors, 2013: *Climate Change 2013: The Physical Science Basis*. [Stocker,
595 T. F., D. Qin, G.-K. Plattner, M. Tignor, S. K. Allen, J. Boschung, A. Nauels, Y. Xia, V. Bex and

596 *P.M. Midgley (eds.)*], chap. 10 Detection and Attribution of climate change: From global to
597 regional, 867–952. Cambridge University Press, doi:10.1017/CBO9781107415324.022.

598 Blessing, S., K. Fraedrich, M. Junge, T. Kunz, and F. Lunkeit, 2005: Daily North-Atlantic Os-
599 cillation (NAO) index: Statistics and its stratospheric polar vortex dependence. *Meteor. Z.*, **14**,
600 763–769, doi:10.1127/0941-2948/2005/0085.

601 Buchan, J., J. J.-M. Hirschi, A. T. Blaker, and B. Sinha, 2014: North Atlantic SST anomalies and
602 the cold North European weather events of winter 2009/10 and December 2010. *Mon. Weather*
603 *Rev.*, **142**, 922–932, doi:10.1175/MWR-D-13-00104.1.

604 Buehler, T., C. C. Raible, and T. F. Stocker, 2011: The relationship of winter season North Atlantic
605 blocking frequencies to extreme cold or dry spells in the ERA-40. *Tellus A*, **63**, 212–222, doi:
606 10.1111/j.1600-0870.2010.00492.x.

607 Burke, C., P. Stott, A. Ciavarella, and Y. Sun, 2016: Attribution of extreme rainfall in south-
608 east China during May 2015. *Bull. Amer. Meteor. Soc.*, **97** (12), S92–S96, doi:10.1175/
609 BAMS-D-16-0144.1.

610 Cattiaux, J., R. Vautard, C. Cassou, P. Yiou, V. Masson-Delmotte, and F. Codron, 2010: Winter
611 2010 in Europe: A cold extreme in a warming climate. *Geophys. Res. Lett.*, **37**, L20 704, doi:
612 10.1029/2010GL044613.

613 Christiansen, B., 2001: Downward propagation of zonal mean zonal wind anomalies from the
614 stratosphere to the troposphere: Model and reanalysis. *J. Geophys. Res.*, **106**, 27 307–27 322.

615 Christiansen, B., 2007: Atmospheric circulation regimes: Can cluster analysis provide the num-
616 ber? *J. Climate*, **20**, 2229–2250.

- 617 Christiansen, B., 2013: Changes in temperature records and extremes: Are they statistically sig-
618 nificant? *J. Climate*, **26**, 7863–7875, doi:10.1175/JCLI-D-12-00814.1.
- 619 Christiansen, B., 2015: The role of the selection problem and non-gaussianity in attribution of
620 single events to climate change. *J. Climate*, **28**, 9873–9891, doi:10.1175/JCLI-D-15-0318.1.
- 621 Christidis, N., M. McCarthy, A. Ciavarella, and P. A. Stott, 2016: Human contribution to the
622 record sunshine of winter 2014/15 in the United Kingdom. *Bull. Amer. Meteor. Soc.*, **97 (12)**,
623 S47–S50, doi:10.1175/BAMS-D-16-0143.1.
- 624 Christidis, N., P. A. Stott, and A. Ciavarella, 2014: The effect of anthropogenic climate change on
625 the cold spring of 2013 in the United Kingdom. *Bull. Amer. Meteor. Soc.*, **95 (9)**, S79–S82.
- 626 Christidis, N., P. A. Stott, A. A. Scaife, A. Arribas, G. S. Jones, D. Copesey, J. R. Knight, and W. J.
627 Tennant, 2013: A new HadGEM3-A-Based system for attribution of weather- and climate-
628 related extreme events. *J. Climate*, **26 (9)**, 2756–2783.
- 629 Ciavarella, A., and Coauthors, 2017: The HadGEM3-A N216 system for probabilistic attribution
630 of extreme weather and climate events. In preparation.
- 631 Cohen, J., J. Foster, M. Barlow, K. Saito, and J. Jones, 2010: Winter 2009–2010: A case
632 study of an extreme Arctic Oscillation event. *Geophys. Res. Lett.*, **37**, L17 707, doi:10.1029/
633 2010GL044256.
- 634 Cohen, J., and Coauthors, 2014: Recent Arctic amplification and extreme mid-latitude weather.
635 *Nat. Geosci.*, **7**, 627, doi:10.1038/ngeo2234.
- 636 Conlon, K. C., N. B. Rajkovich, J. L. White-Newsome, L. Larsen, and M. S. O’Neill, 2011:
637 Preventing cold-related morbidity and mortality in a changing climate. *Maturitas*, **69**, 197–202,
638 doi:10.1016/j.maturitas.2011.04.004.

639 Coumou, D., and S. Rahmstorf, 2012: A decade of weather extremes. *Nat. Clim. Change*, **2**,
640 491–496, doi:10.1038/nclimate1452.

641 de Vries, H., R. J. Haarsma, and W. Hazeleger, 2012: Western European cold spells in current and
642 future climate. *Geophys. Res. Lett.*, **39**, L04 706, doi:10.1029/2011GL050665.

643 Doll, C., C. Trinks, N. Sedlacek, V. Pelikan, T. Comes, and F. Schultmann, 2014: Adapting rail
644 and road networks to weather extremes: case studies for southern Germany and Austria. *Natural*
645 *Hazards*, **72**, 63–85, doi:10.1007/s11069-013-0969-3.

646 Eden, J. M., K. Wolter, F. E. L. Otto, and G. J. v. Oldenborgh, 2016: Multi-method attribution
647 analysis of extreme precipitation in Boulder, Colorado. *Environ. Res. Lett.*, **11**, 124 009, doi:
648 10.1088/1748-9326/11/12/124009.

649 Field, C. B., and Coauthors, 2012: Managing the risks of extreme events and disasters to advance
650 climate change adaptation. *A Special Report of Working Groups I and II of the Intergovernmen-*
651 *tal Panel on Climate Change Cambridge University Press, Cambridge, UK, and New York, NY,*
652 *USA.*

653 Fischer, E. M., and R. Knutti, 2015: Anthropogenic contribution to global occurrence of heavy-
654 precipitation and high-temperature extremes. *Nat. Clim. Change*, **5 (6)**, 560–564, doi:10.1038/
655 nclimate2617.

656 Francis, J. A., 2017: Why are Arctic linkages to extreme weather still up in the air? *Bull. Amer.*
657 *Meteor. Soc.*, doi:10.1175/BAMS-D-17-0006.1.

658 Francis, J. A., W. Chan, D. J. Leathers, J. R. Miller, and D. E. Veron, 2009: Winter Northern
659 Hemisphere weather patterns remember summer Arctic sea-ice extent. *Geophys. Res. Lett.*, **36**,
660 L07 503, doi:10.1029/2009GL037274.

661 Frich, P., L. V. Alexander, P. Della-Marta, B. Gleason, M. Haylock, A. M. G. Klein Tank, and
662 T. Peterson, 2002: Observed coherent changes in climatic extremes during the second half of
663 the twentieth century. *Clim. Res.*, **19** (3), 193–212.

664 Gao, Y., and Coauthors, 2014: Arctic sea ice and Eurasian climate: A review. *Adv. Atmos. Sci.*, **32**,
665 92–114, doi:10.1007/s00376-014-0009-6.

666 Gerber, F., J. Sedláček, and R. Knutti, 2014: Influence of the western North Atlantic and the
667 Barents Sea on European winter climate. *Geophys. Res. Lett.*, **41**, 561–567, doi:10.1002/
668 2013GL058778.

669 Greatbatch, R. J., 2000: The North Atlantic Oscillation. *Stoch. Environ. Res. Risk Assess.*, **14**,
670 213–242, doi:10.1007/s004770000047.

671 Hannart, A., J. Pearl, F. E. L. Otto, P. Naveau, and M. Ghil, 2015: Causal counterfactual theory
672 for the attribution of weather and climate-related events. *Bull. Amer. Meteor. Soc.*, doi:10.1175/
673 BAMS-D-14-00034.1.

674 Hansen, G., M. Auffhammer, and A. R. Solow, 2014: On the attribution of a single event to climate
675 change. *J. Climate*, **27** (22), 8297–8301, doi:10.1175/JCLI-D-14-00399.1.

676 Haylock, M. R., N. Hofstra, A. M. G. Klein Tank, E. J. Klok, P. D. Jones, and M. New, 2008:
677 A European daily high-resolution gridded data set of surface temperature and precipitation for
678 1950–2006. *J. Geophys. Res.*, **113**, D20 119, doi:10.1029/2008JD010201.

679 Jung, T., F. Vitart, L. Ferranti, and J.-J. Morcrette, 2011: Origin and predictability of the
680 extreme negative NAO winter of 2009/10. *Geophys. Res. Lett.*, **38**, L07 701, doi:10.1029/
681 2011GL046786.

682 Kalnay, E., and Coauthors, 1996: The NCEP/NCAR 40-year reanalysis project. *Bull. Am. Meteo-*
683 *rol. Soc.*, **77**, 437–471.

684 Li, C., B. Stevens, and J. Marotzke, 2015: Eurasian winter cooling in the warming hiatus of 1998-
685 2012. *Geophys. Res. Lett.*, **42**, 2015GL065 327, doi:10.1002/2015GL065327.

686 Liu, J., J. A. Curry, H. Wang, M. Song, and R. M. Horton, 2012: Impact of declining Arctic
687 sea ice on winter snowfall. *Proc. Natl. Acad. Sci. USA*, **109**, 4074–4079, doi:10.1073/pnas.
688 1114910109.

689 Meehl, G. A., C. Tebaldi, G. Walton, D. Easterling, and L. McDaniel, 2009: Relative increase of
690 record high maximum temperatures compared to record low minimum temperatures in the US.
691 *Geophys. Res. Lett.*, **36**, L23 701.

692 Mori, M., M. Watanabe, H. Shiogama, J. Inoue, and M. Kimoto, 2014: Robust Arctic sea-ice
693 influence on the frequent Eurasian cold winters in past decades. *Nat. Geosci.*, **7**, 869, doi:10.
694 1038/ngeo2277.

695 National Academies of Sciences, Engineering, and Medicine, 2016: *Attribution of Extreme*
696 *Weather Events in the Context of Climate Change*. The National Academies Press, Washing-
697 ton, DC, doi:10.17226/21852.

698 Orsolini, Y. J., R. Senan, R. E. Benestad, and A. Melsom, 2011: Autumn atmospheric response
699 to the 2007 low Arctic sea ice extent in coupled ocean-atmosphere hindcasts. *Clim. Dyn.*, **38**,
700 2437–2448, doi:10.1007/s00382-011-1169-z.

701 Otto, F. E. L., E. Boyd, R. G. Jones, R. J. Cornforth, R. James, H. R. Parker, and M. R. Allen,
702 2015: Attribution of extreme weather events in Africa: a preliminary exploration of the science
703 and policy implications. *Clim. Change.*, 1–13, doi:10.1007/s10584-015-1432-0.

704 Ouzeau, G., J. Cattiaux, H. Douville, A. Ribes, and D. Saint-Martin, 2011: European cold winter
705 2009-2010: How unusual in the instrumental record and how reproducible in the ARPEGE-
706 Climat model? *Geophys. Res. Lett.*, **38**, L11 706, doi:10.1029/2011GL047667.

707 Overland, J., J. A. Francis, R. Hall, E. Hanna, S.-J. Kim, and T. Vihma, 2015: The melting Arctic
708 and midlatitude weather patterns: Are they connected? *J. Climate*, **28**, 7917–7932, doi:10.1175/
709 JCLI-D-14-00822.1.

710 Overland, J. E., and M. Wang, 2010: Large-scale atmospheric circulation changes are associated
711 with the recent loss of Arctic sea ice. *Tellus A*, **62**, 1–9, doi:10.1111/j.1600-0870.2009.00421.x.

712 Peterson, T. C., P. A. Stott, and S. Herring, 2012: Explaining extreme events of 2011 from a climate
713 perspective. *Bull. Amer. Meteor. Soc.*, **93**, 1041–1067, doi:10.1175/BAMS-D-12-00021.1.

714 Petoukhov, V., and V. A. Semenov, 2010: A link between reduced Barents-Kara sea ice and
715 cold winter extremes over northern continents. *J. Geophys. Res.*, **115**, D21 111, doi:10.1029/
716 2009JD013568.

717 Prichard, D., and J. Theiler, 1994: Generating surrogate data for time series with several simultane-
718 ously measured variables. *Phys. Rev. Lett.*, **73** (7), 951–954, doi:10.1103/PhysRevLett.73.951.

719 Rayner, N. A., D. E. Parker, E. B. Horton, C. K. Folland, L. V. Alexander, D. P. Rowell, E. C.
720 Kent, and A. Kaplan, 2003: Global analyses of sea surface temperature, sea ice, and night
721 marine air temperature since the late nineteenth century. *J. Geophys. Res.*, **108** (D14), 4407,
722 doi:10.1029/2002JD002670.

723 Screen, J. A., 2017: The missing Northern European winter cooling response to Arctic sea ice
724 loss. *Nat. Commun.*, **8**, 14 603, doi:10.1038/ncomms14603.

725 Sévellec, F., A. V. Fedorov, and W. Liu, 2017: Arctic sea-ice decline weakens the Atlantic Merid-
726 ional Overturning Circulation. *Nat. Clim. Change*, **7**, 604, doi:10.1038/nclimate3353.

727 Stott, P. A., D. A. Stone, and M. R. Allen, 2004: Human contribution to the European heatwave
728 of 2003. *Nature*, **432**, 610–614, doi:10.1038/nature03089.

729 Stott, P. A., and Coauthors, 2013: Attribution of weather and climate-related events. *Climate*
730 *Science for Serving Society*, G. R. Asrar, and J. W. Hurrell, Eds., Springer Netherlands, 307–
731 337, URL http://link.springer.com/chapter/10.1007/978-94-007-6692-1_12.

732 Tang, Q., X. Zhang, X. Yang, and J. A. Francis, 2013: Cold winter extremes in northern continents
733 linked to Arctic sea ice loss. *Environ. Res. Lett.*, **8**, 014036, doi:10.1088/1748-9326/8/1/014036.

734 Taylor, K. E., R. J. Stouffer, and G. A. Meehl, 2011: An overview of CMIP5 and the experiment
735 design. *Bull. Am. Meteorol. Soc.*, **93**, 485–498, doi:10.1175/BAMS-D-11-00094.1.

736 Theiler, J., S. Eubank, A. Longtin, B. Galdrikian, and J. Doyne Farmer, 1992: Testing for non-
737 linearity in time series: the method of surrogate data. *Physica D*, **58**, 77–94, doi:10.1016/
738 0167-2789(92)90102-S.

739 Twardosz, R., and U. Kossowska-Cezak, 2016: Exceptionally cold and mild winters in Europe
740 (1951–2010). *Theor. Appl. Climatol.*, **125**, 399–411, doi:10.1007/s00704-015-1524-9.

741 Uppala, S. M., and Coauthors, 2005: The ERA-40 re-analysis. *Quart. J. Roy. Meteor. Soc.*, **131**,
742 2961–3012.

743 van der Schrier, G., E. J. M. van den Besselaar, A. M. G. Klein Tank, and G. Verver, 2013:
744 Monitoring European average temperature based on the E-OBS gridded data set. *J. Geophys.*
745 *Res.*, **118**, 5120–5135, doi:10.1002/jgrd.50444.

746 Van Oldenborgh, G. J., R. Haarsma, H. De Vries, and M. R. Allen, 2014: Cold extremes in North
747 America vs. mild weather in Europe: The winter of 2013–14 in the context of a warming world.
748 *Bull. Amer. Meteor. Soc.*, **96**, 707–714, doi:10.1175/BAMS-D-14-00036.1.

749 Vargin, P., 2015: Stratospheric polar vortex splitting in December 2009. *Atmos.-Ocean*, **53**, 29–41,
750 doi:10.1080/07055900.2013.851066.

751 Vautard, R., and Coauthors, 2017: Evaluation of the HadGEM3-A simulations in view of detection
752 and attribution of human influence on extreme events in Europe. *Clim. Dyn.*, *under review*.

753 Vihma, T., 2014: Effects of Arctic sea ice decline on weather and climate: A review. *Surveys in*
754 *Geophysics*, **35**, 1175–1214, doi:10.1007/s10712-014-9284-0.

755 Walters, D., and Coauthors, 2016: The Met Office Unified Model Global Atmosphere 6.0/6.1
756 and JULES Global Land 6.0/6.1 configurations. *Geosci. Model Dev. Discuss.*, **2016**, 1–52, doi:
757 10.5194/gmd-2016-194.

758 Wang, C., H. Liu, and S.-K. Lee, 2010: The record-breaking cold temperatures during the winter
759 of 2009/2010 in the Northern Hemisphere. *Atmos. Sci. Lett.*, **11**, 161–168, doi:10.1002/asl.278.

760 WMO, 2010: Assessment of the observed extreme conditions during the 2009/2010 boreal winter.
761 Tech. Rep. TD-1550, World Meteorological Organization.

762 Yang, S., and J. H. Christensen, 2012: Arctic sea ice reduction and European cold win-
763 ters in CMIP5 climate change experiments. *Geophys. Res. Lett.*, **39**, L20707, doi:10.1029/
764 2012GL053338.

765 Yiou, P., D. Dacunha-Castelle, S. Parey, and T. T. Huong Hoang, 2009: Statistical representation
766 of temperature mean and variability in Europe. *Geophys. Res. Lett.*, **36**, L04710, doi:10.1029/
767 2008GL036836.

768 Zhang, X., C. Lu, and Z. Guan, 2012: Weakened cyclones, intensified anticyclones and recent
769 extreme cold winter weather events in Eurasia. *Environ. Res. Lett.*, **7**, 044 044, doi:10.1088/
770 1748-9326/7/4/044044.

771 **LIST OF FIGURES**

772 **Fig. 1.** Blob index as function of time. The blob index is the area of the largest continuous region
773 with temperature anomalies below -2σ , where σ is the local, seasonally varying standard
774 deviation. It is normalized with the total area of the considered region. First panel: Winter
775 2009-2010 from E-OBS. Second panel: 1960-2013 from E-OBS. Third panel: 1960-2013
776 from a historical HadGEM3-A ensemble member. Fourth panel: 1960-2013 from a per-
777 turbed surrogate ensemble member. Three lowest panels include all year. 39

778 **Fig. 2.** The temperature of 19th Dec. 2009 which is the winter day of 2009-2010 with the largest
779 blob index. Top left: Temperature [$^{\circ}\text{C}$]. Top right: Anomaly after removing annual cycle
780 [$^{\circ}\text{C}$]. Bottom: Anomaly normalized with seasonal standard deviation. 40

781 **Fig. 3.** Left: Temperature [$^{\circ}\text{C}$] of the coldest day in winter 2009-2010 found individually for each
782 grid-point. Right: Fraction of winters in 1960-2013 with days colder than the coldest day in
783 winter 2009-2010. 41

784 **Fig. 4.** European mean winter temperatures [$^{\circ}\text{C}$] as function of time. Top: HadGEM3-A. Bottom:
785 Surrogate. Observations: blue curve. Historical and perturbed ensembles: black curves,
786 Histnat and unperturbed ensembles: red curves. Ensemble means shown with thick curves. . . . 42

787 **Fig. 5.** Local daily winter temperatures have been normalized with their seasonally varying standard
788 deviation and pooled. Left panel shows the distribution as function of time. Contour levels
789 are 0.0001, 0.001, 0.01, 0.05, 0.1, 0.2, 0.3, 0.4, and 0.5. Right panel shows the distributions
790 before (light shading) and after (dark shading) 1985. From top: Observations (E-OBS),
791 HadGEM3-A historical, and perturbed surrogate. 43

792 **Fig. 6.** Return periods of the blob index (largest continuous area) for winter. Black: observations.
793 Blue: surrogates. Red: HadGEM3-A. Thin curves are individual ensemble members, thick
794 curves are pooled ensembles. Only historical and perturbed ensembles shown. 44

795 **Fig. 7.** Top: Long term winter means of grid-point temperatures in observations and historical
796 HadGEM3-A. Bottom left: Model bias. Differences in long term mean between HadGEM3-
797 A historical and observations. Bottom right: Differences in long term mean between
798 HadGEM3-A historical and histnat. Unit: [$^{\circ}\text{C}$]. Large dots where differences are estimated
799 to be statistically significant at the 5 % level. 45

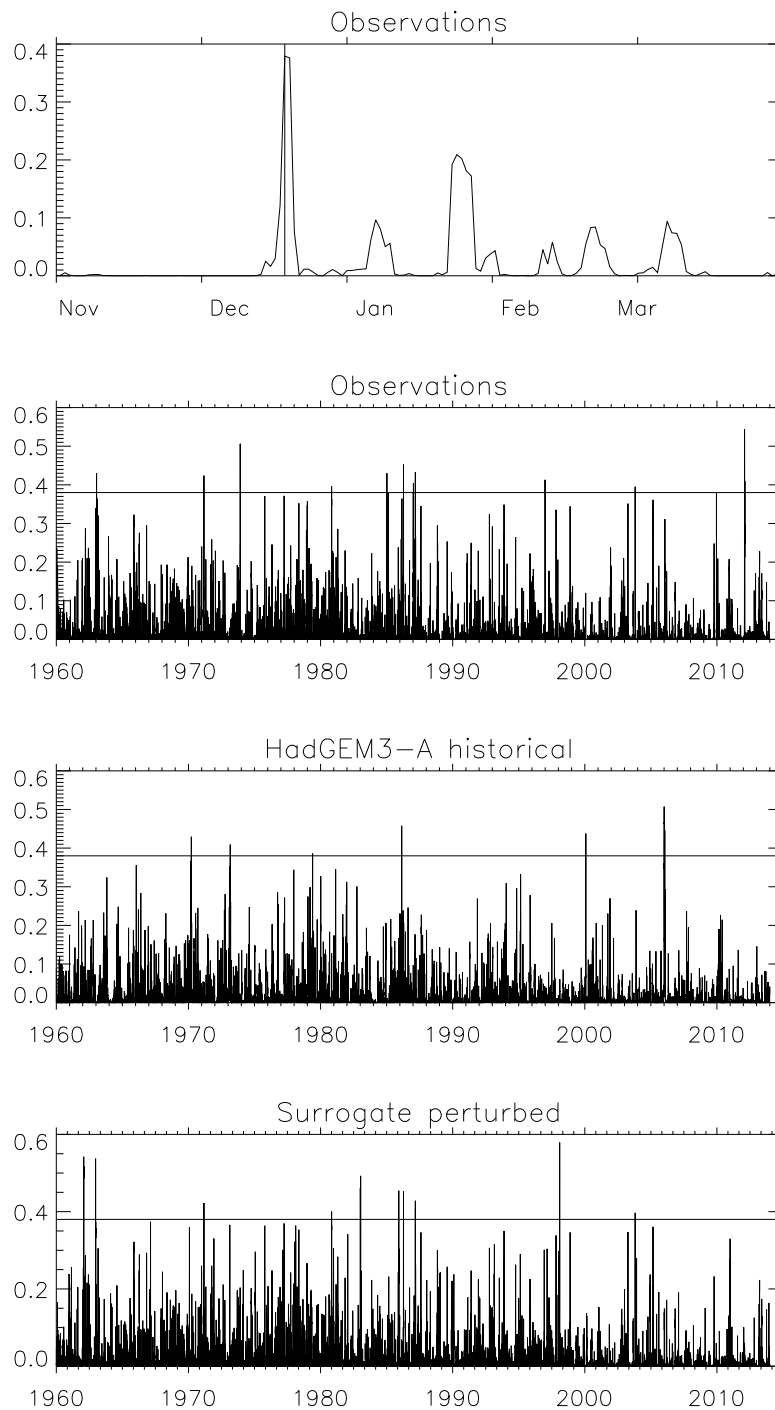
800 **Fig. 8.** Linear trends of grid-point temperatures in winter [$^{\circ}\text{C}/\text{decade}$]. Top: Observations. Middle:
801 Historical and histnat HadGEM3-A. Bottom: Perturbed and unperturbed surrogate. Large
802 dots where trends are estimated to be statistically significant at the 5 % level. 46

803 **Fig. 9.** Standard deviation of winter anomalies of grid-point temperatures [$^{\circ}\text{C}$]. Top: Observa-
804 tions. Middle: Historical HadGEM3-A and perturbed surrogate. Bottom: Difference be-
805 tween historical HadGEM3-A and observations and difference between historical and hist-
806 nat HadGEM3-A. Large dots where differences are estimated to be statistically significant
807 at the 5 % level. 47

808 **Fig. 10.** As Fig. 9 but for skewness of winter anomalies of grid-point temperatures. 48

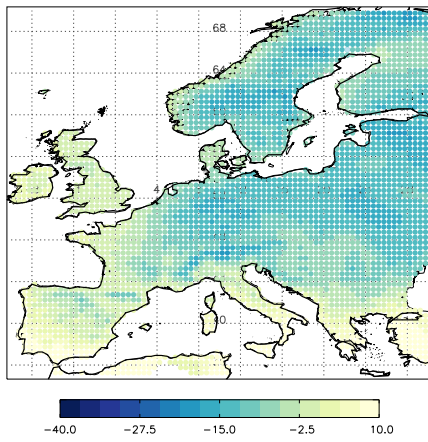
809 **Fig. 11.** As Fig. 9 but for the 5 % quantile of winter anomalies of grid-point temperatures [$^{\circ}\text{C}$]. 49

- 810 **Fig. 12.** Time development for spatial mean of temperature [$^{\circ}\text{C}$], standard deviation [$^{\circ}\text{C}$], and skewness. Standard deviation and skewness calculated from anomalies. Observations (green),
811 HadGEM3-A historical (orange), surrogate perturbed (cyan). 50
812
- 813 **Fig. 13.** The distributions of the temperatures [$^{\circ}\text{C}$] of the coldest day in winter for grid-points near
814 Utrecht and Oslo. Based on 15*53 winters. Historical or perturbed climate: light shading.
815 Histnat or unperturbed climate: dark shading. Thin vertical gray lines are the observed
816 winters. Green vertical line is the observed winter 2009-2010. Orange vertical line is this
817 winter corrected with mean bias. Risk ratios are provided at the top of the panels. For the
818 HadGEM3-A the second number includes bias correction. 51
- 819 **Fig. 14.** Maps of the risk ratios of the temperature of the coldest day in the winter 2009-2010. Den-
820 sities calculated over all winter days. Left: HadGEM3-A. Right: Surrogate method. Top:
821 based on the full period 1960-2013. Bottom: Based on 1985-2013. Large dots where the
822 ratio is estimated to be significantly different from 1 (5 % level). 52
- 823 **Fig. 15.** The risk ratio (thick black curve) for the blob index, i.e., the largest continuous area with
824 temperature anomalies less than -2σ . Vertical green line: observed value for winter 2009-
825 2001. Thin black curves: bootstraps. Black dashed curves: 95 % confidence interval. Left:
826 HadGEM3-A. Right: Surrogate method. Top: based on the full period 1960-2013. Middle:
827 Based on 1985-2013. Bottom: Based on 2007-2012. 53
- 828 **Fig. A1.** First row: Probability densities of the largest value, x_{max} , of n independent and identically
829 distributed variables for $n = 1$ and $n = 100$. Cyan: the unperturbed case, p_1^{uc} and p_{100}^{uc} .
830 Red: under climate change, p_1^{pc} and p_{100}^{pc} . The perturbed and unperturbed cases related by
831 $p_1^{pc}(x) = p_1^{uc}(x - c)$, $c = 0.3$. These curves are shown in logarithmic scale in Fig. S4 in the
832 supplement. Second, third and fourth rows: The ratio of probabilities p_n^{pc}/p_n^{uc} , the risk ratios
833 $RR = (1 - P_n^{pc})/(1 - P_n^{uc})$, and the FARs $\frac{(1 - P_n^{pc}) - (1 - P_n^{uc})}{(1 - P_n^{pc})} = 1 - 1/RR$ as function of x_{max} . In
834 left panel p_1^{uc} is Gaussian, in right panel it is t-distributed with 5 degrees of freedom. In each
835 panel are shown results for $n=1$ (blue), 10 (green), 100 (orange), 1000 (red), 10000 (black). 54
- 836 **Fig. A2.** As for Fig. A1 but with the perturbed climate given by $p_1^{pc}(x) = p_1^{uc}(x + c)$, $c = 0.3$, indi-
837 cating fewer positive extremes in the perturbed climate. 55

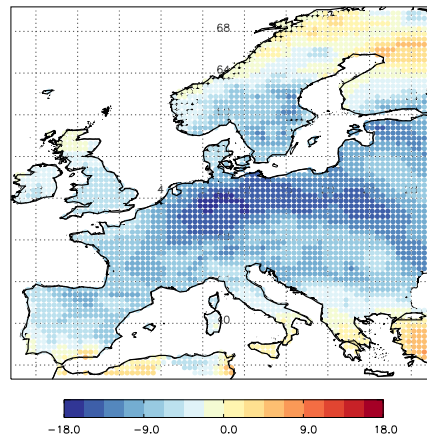


838 FIG. 1. Blob index as function of time. The blob index is the area of the largest continuous region with
 839 temperature anomalies below -2σ , where σ is the local, seasonally varying standard deviation. It is normalized
 840 with the total area of the considered region. First panel: Winter 2009-2010 from E-OBS. Second panel: 1960-
 841 2013 from E-OBS. Third panel: 1960-2013 from a historical HadGEM3-A ensemble member. Fourth panel:
 842 1960-2013 from a perturbed surrogate ensemble member. Three lowest panels include all year.

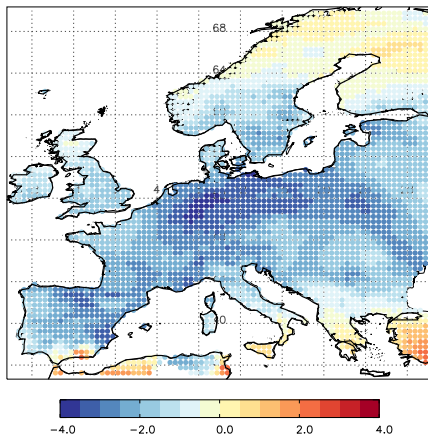
Temperature



Temperature anomaly

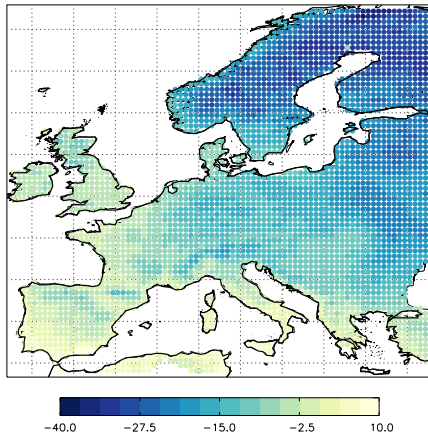


Normalized anomaly

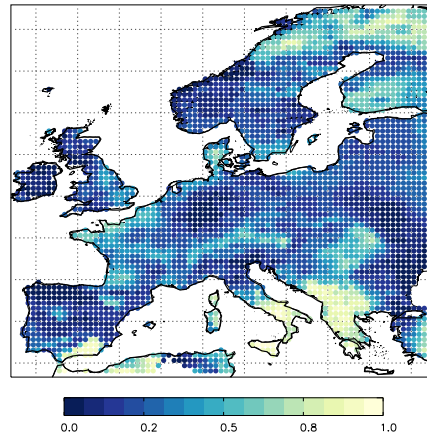


843 FIG. 2. The temperature of 19th Dec. 2009 which is the winter day of 2009-2010 with the largest blob
844 index. Top left: Temperature [$^{\circ}\text{C}$]. Top right: Anomaly after removing annual cycle [$^{\circ}\text{C}$]. Bottom: Anomaly
845 normalized with seasonal standard deviation.

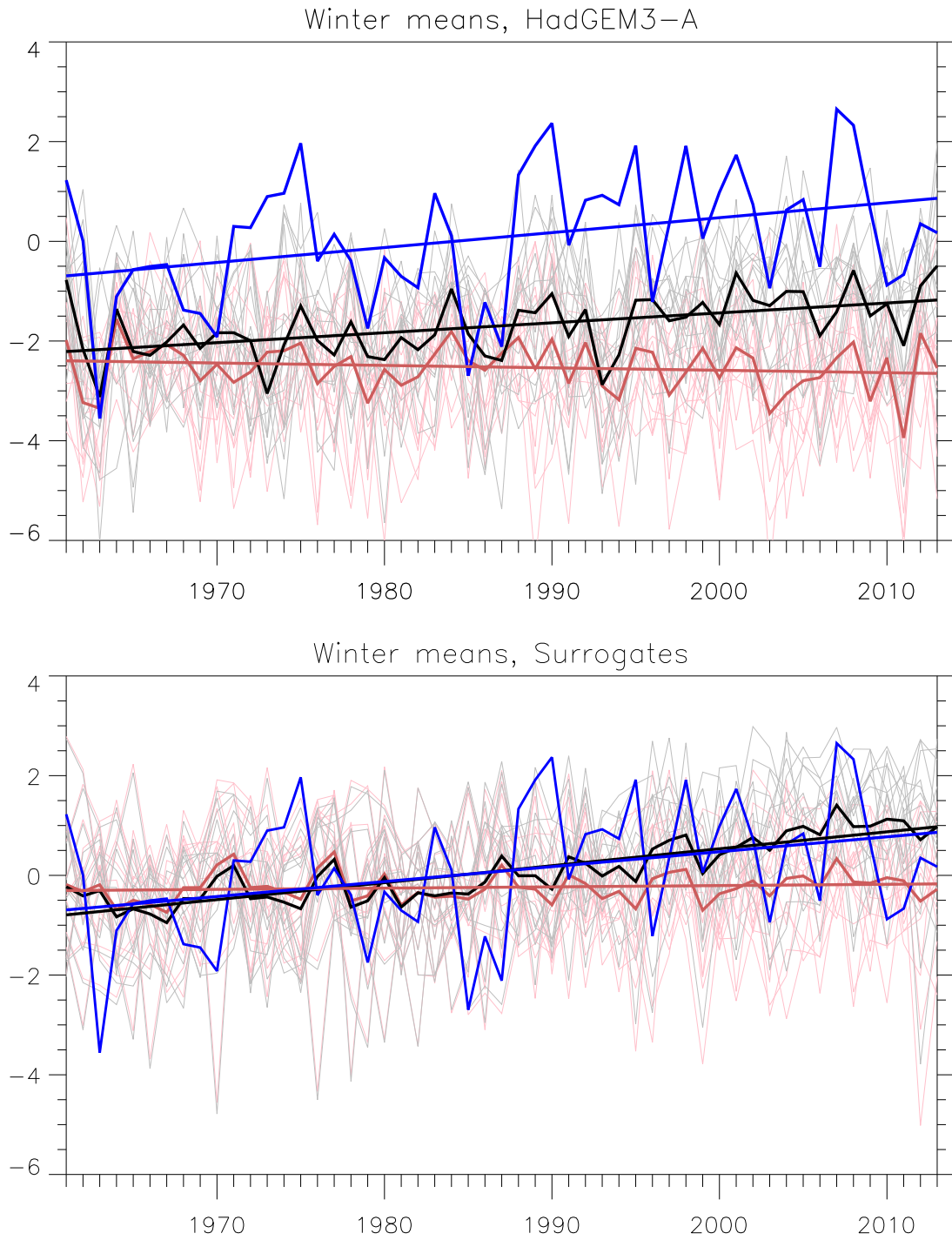
Coldest day 2009–2010



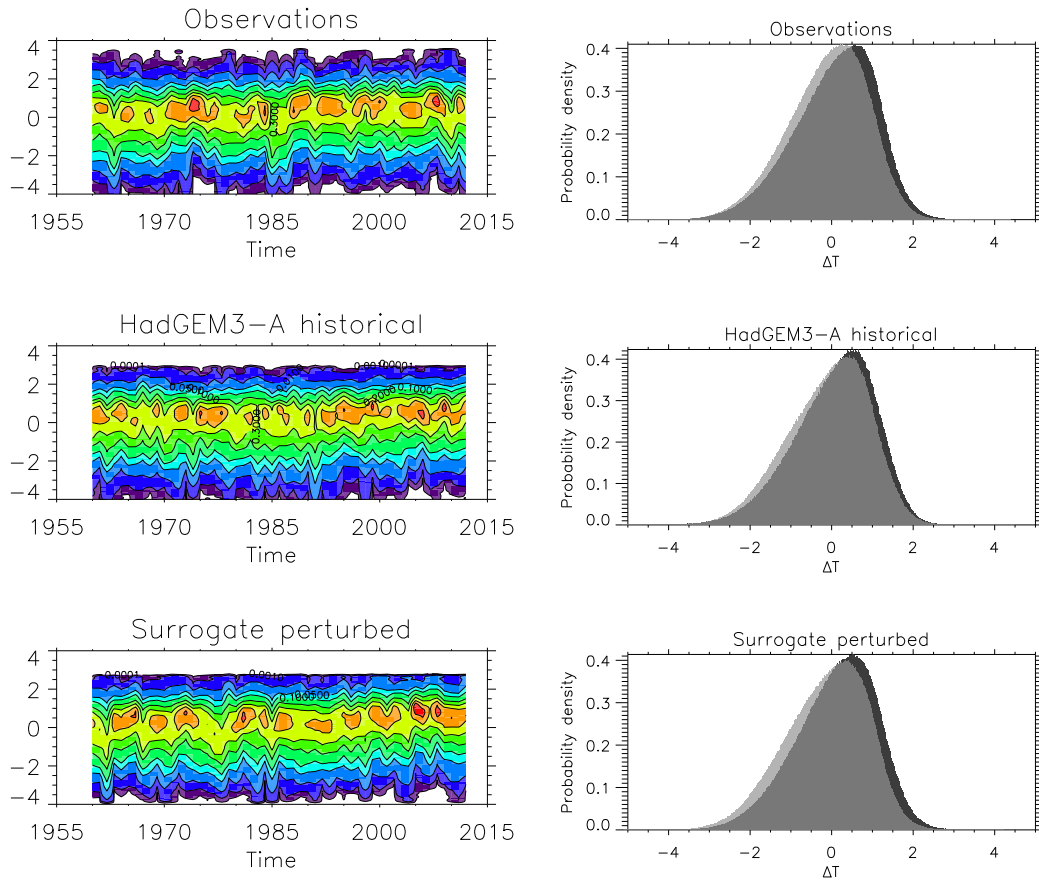
Fraction of winters colder than 2009–2010



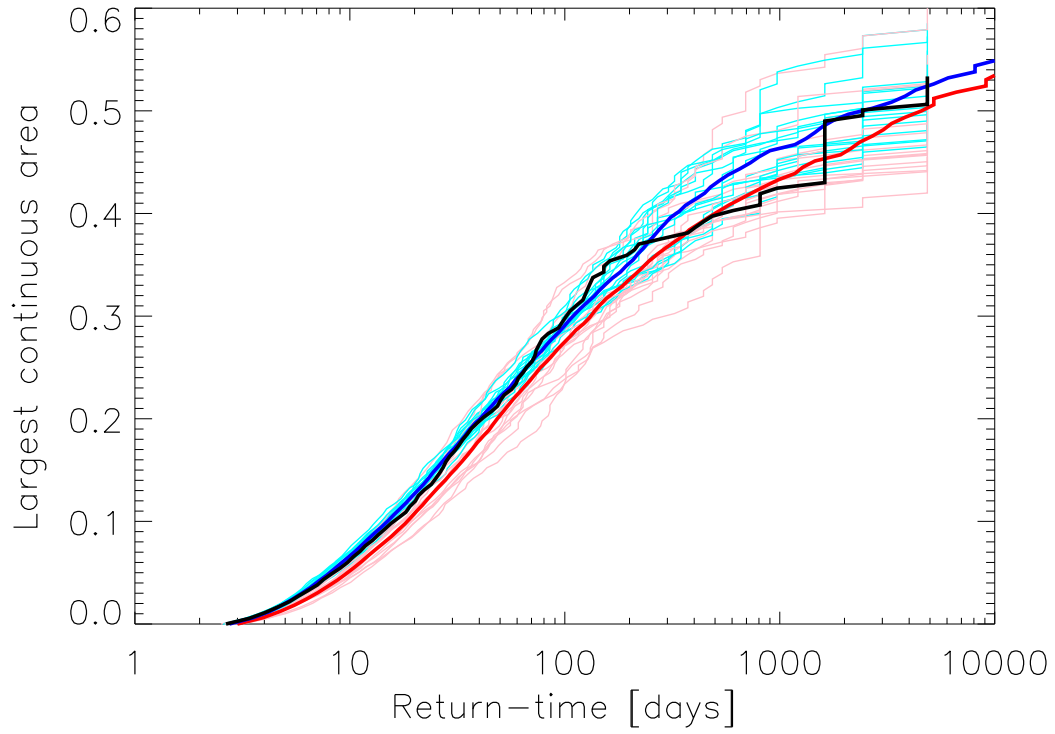
846 FIG. 3. Left: Temperature [$^{\circ}\text{C}$] of the coldest day in winter 2009-2010 found individually for each grid-point.
847 Right: Fraction of winters in 1960-2013 with days colder than the coldest day in winter 2009-2010.



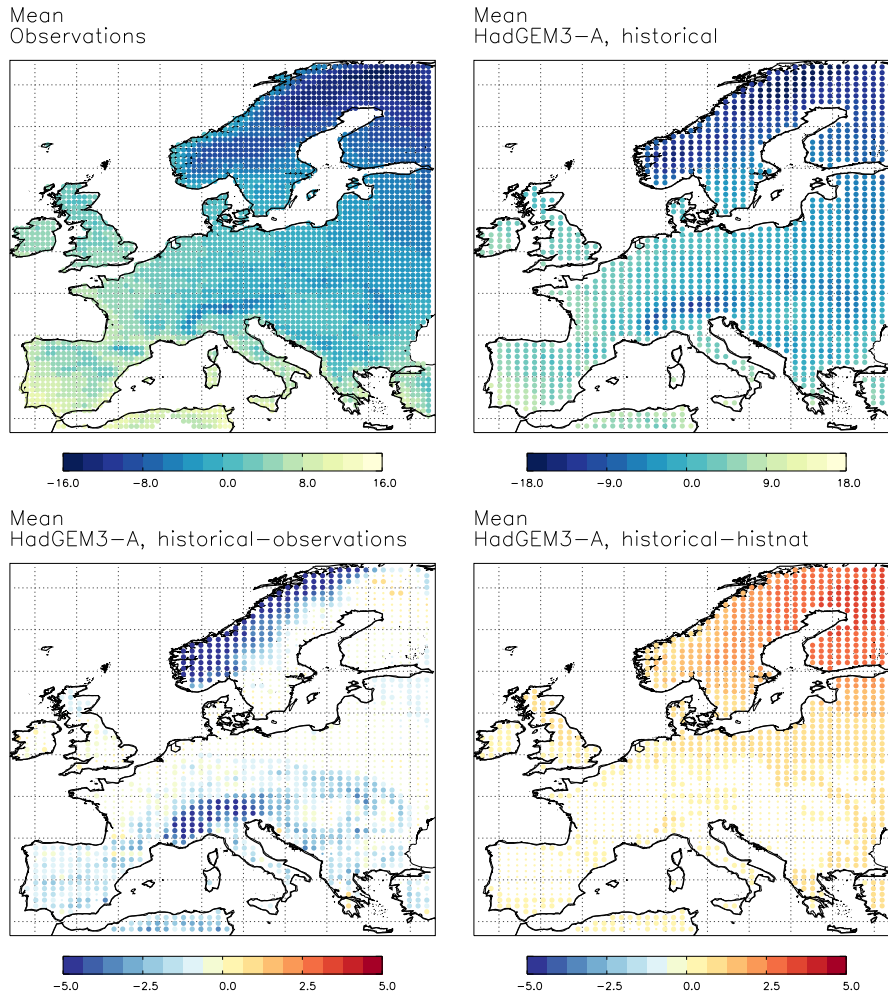
848 FIG. 4. European mean winter temperatures [$^{\circ}\text{C}$] as function of time. Top: HadGEM3-A. Bottom: Surrogate.
 849 Observations: blue curve. Historical and perturbed ensembles: black curves, Histnat and unperturbed ensembles:
 850 red curves. Ensemble means shown with thick curves.



851 FIG. 5. Local daily winter temperatures have been normalized with their seasonally varying standard deviation
 852 and pooled. Left panel shows the distribution as function of time. Contour levels are 0.0001, 0.001, 0.01, 0.05,
 853 0.1, 0.2, 0.3, 0.4, and 0.5. Right panel shows the distributions before (light shading) and after (dark shading)
 854 1985. From top: Observations (E-OBS), HadGEM3-A historical, and perturbed surrogate.

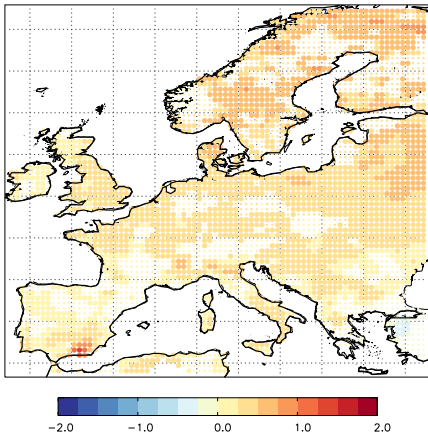


855 FIG. 6. Return periods of the blob index (largest continuous area) for winter. Black: observations. Blue: sur-
856 rogates. Red: HadGEM3-A. Thin curves are individual ensemble members, thick curves are pooled ensembles.
857 Only historical and perturbed ensembles shown.

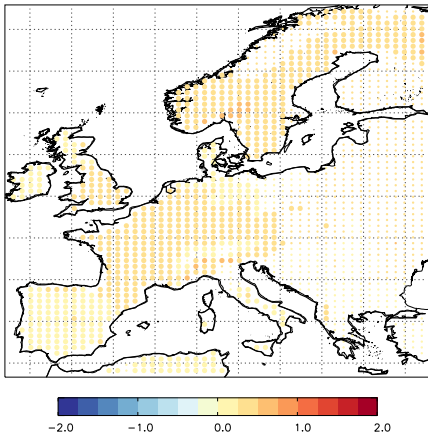


858 FIG. 7. Top: Long term winter means of grid-point temperatures in observations and historical HadGEM3-A.
 859 Bottom left: Model bias. Differences in long term mean between HadGEM3-A historical and observations.
 860 Bottom right: Differences in long term mean between HadGEM3-A historical and histnat. Unit: [°C]. Large
 861 dots where differences are estimated to be statistically significant at the 5 % level.

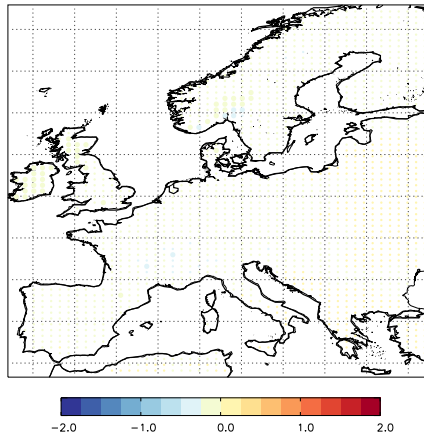
Trend
Observations



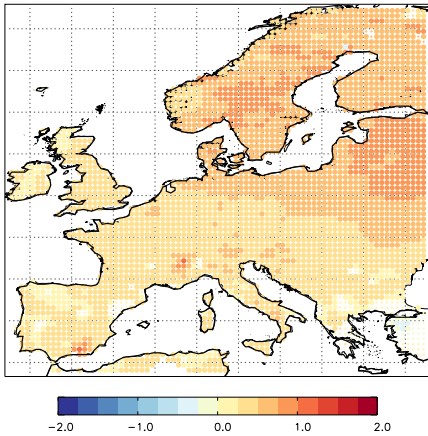
Trend
HadGEM3-A, historical



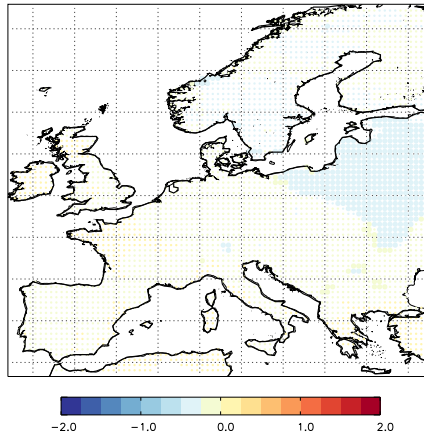
Trend
HadGEM3-A, histnat



Trend
Surrogate, perturbed

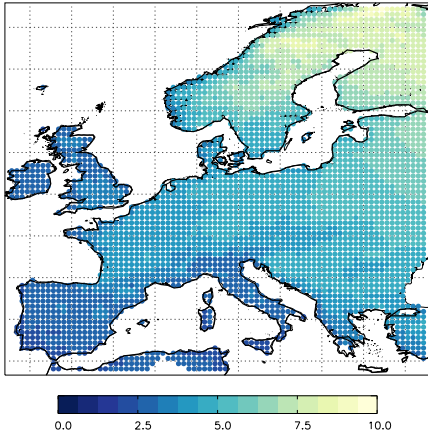


Trend
Surrogate, unperturbed

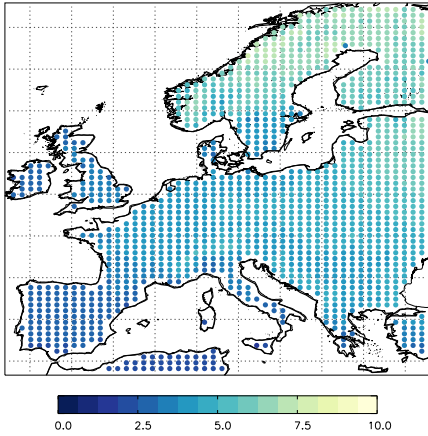


862 FIG. 8. Linear trends of grid-point temperatures in winter [$^{\circ}\text{C}/\text{decade}$]. Top: Observations. Middle: Historical
863 and histnat HadGEM3-A. Bottom: Perturbed and unperturbed surrogate. Large dots where trends are estimated
864 to be statistically significant at the 5 % level.

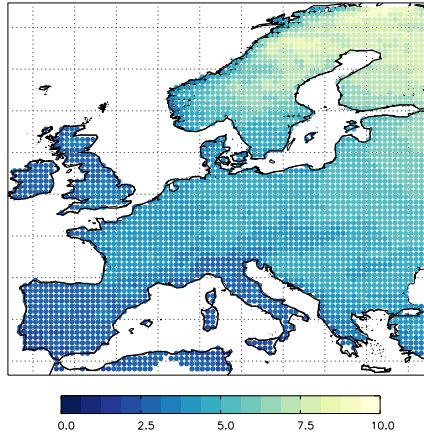
Std. dev., anomalies
Observations



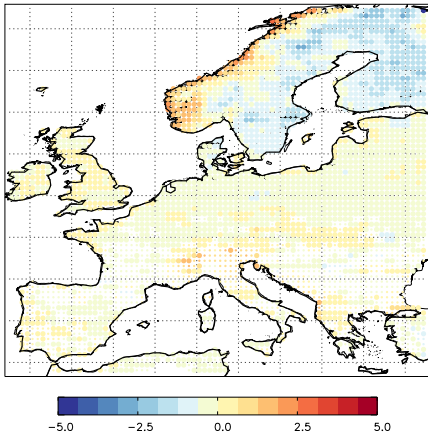
Std. dev., anomalies
HadGEM3-A, historical



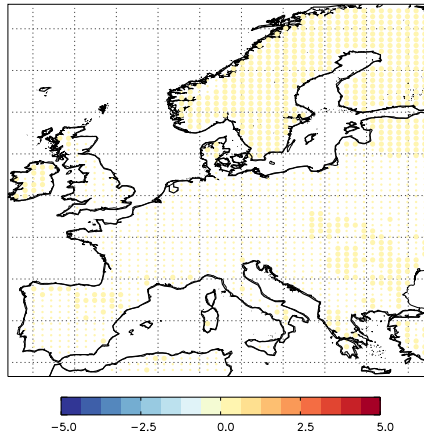
Std. dev., anomalies
Surrogate, perturbed



Std. dev., anomalies
HadGEM3-A, historical-observations

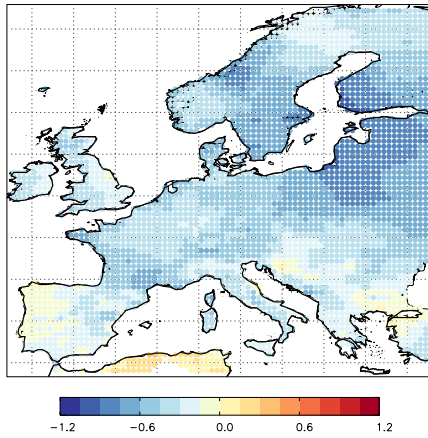


Std. dev., anomalies
HadGEM3-A, historical-histnat

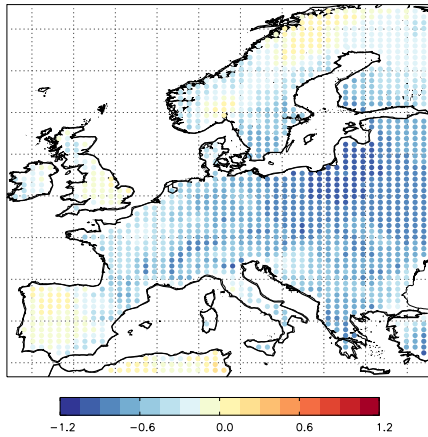


865 FIG. 9. Standard deviation of winter anomalies of grid-point temperatures [$^{\circ}\text{C}$]. Top: Observations. Mid-
866 dle: Historical HadGEM3-A and perturbed surrogate. Bottom: Difference between historical HadGEM3-A
867 and observations and difference between historical and histnat HadGEM3-A. Large dots where differences are
868 estimated to be statistically significant at the 5 % level.

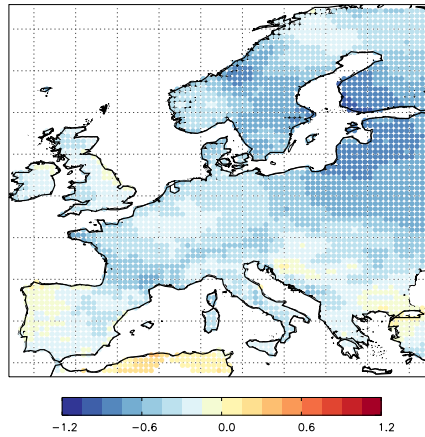
Skewness, anomalies
Observations



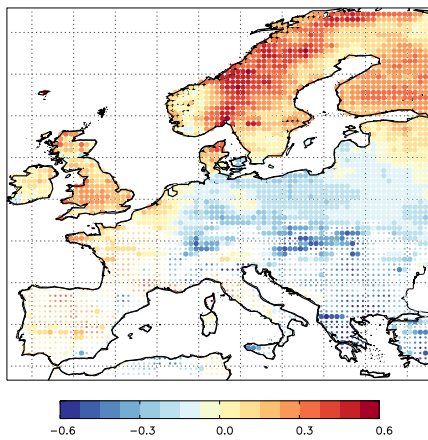
Skewness, anomalies
HadGEM3-A, historical



Skewness,, anomalies
Surrogate, perturbed



Skewness, anomalies
HadGEM3-A, historical-observations



Skewness, anomalies
HadGEM3-A, historical-histnat

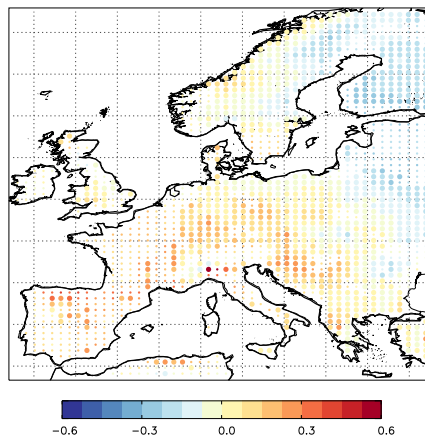
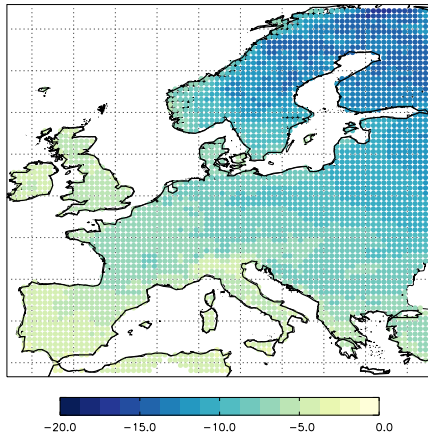
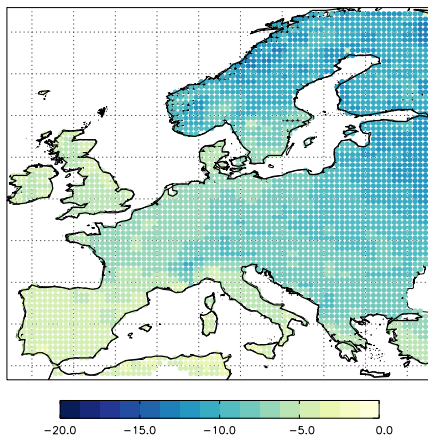


FIG. 10. As Fig. 9 but for skewness of winter anomalies of grid-point temperatures.

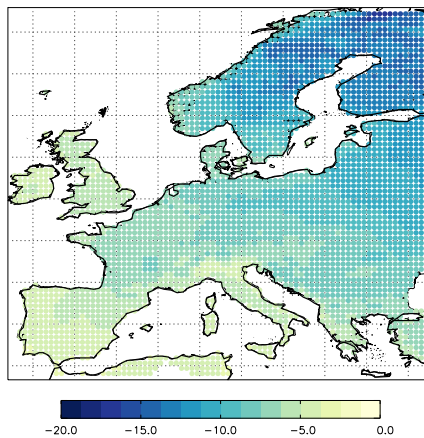
5 % quantile, anomalies
Observations



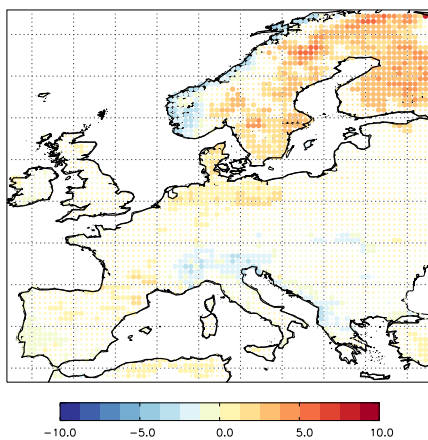
5 % quantile, anomalies
HadGEM3-A, historical



5 % quantile, anomalies
Surrogate, perturbed



5 % quantile, anomalies
HadGEM3-A, historical-observations



5 % quantile, anomalies
HadGEM3-A, historical-histnat

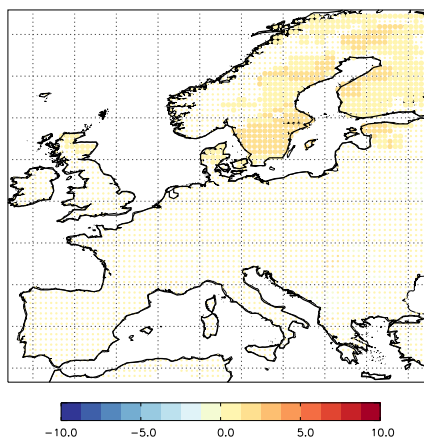
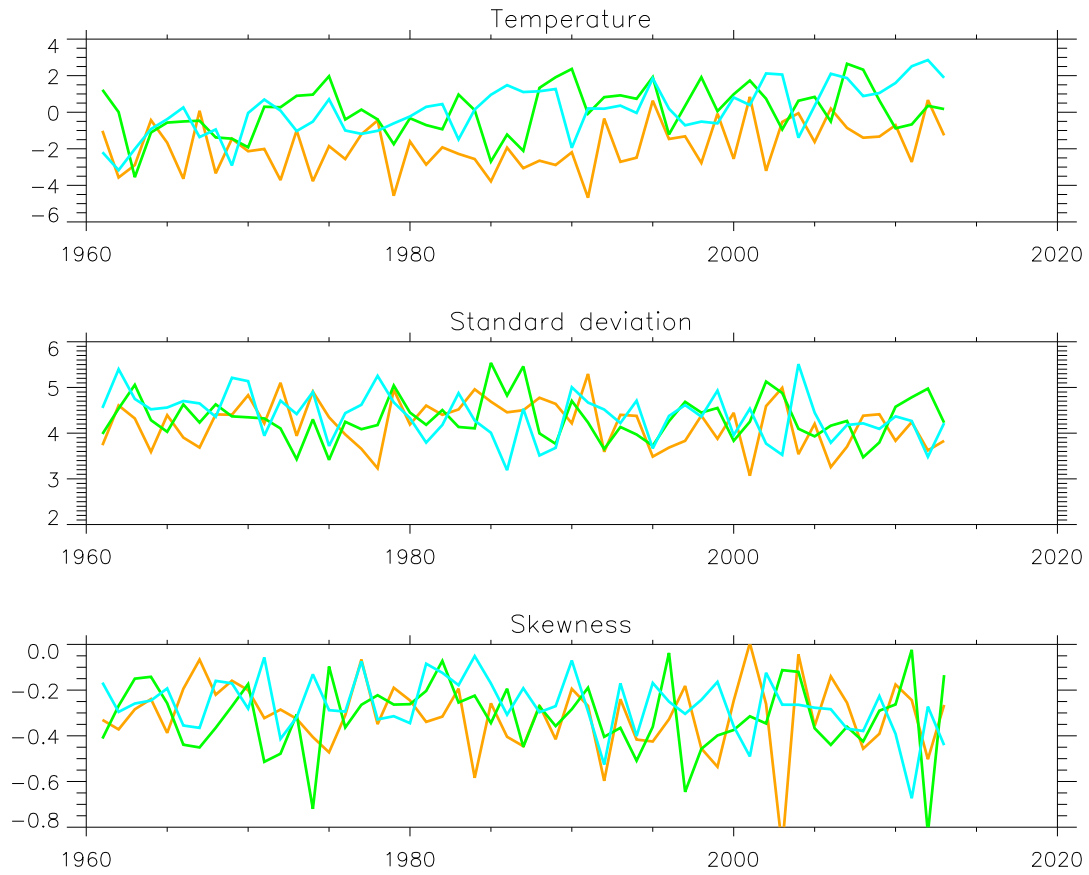
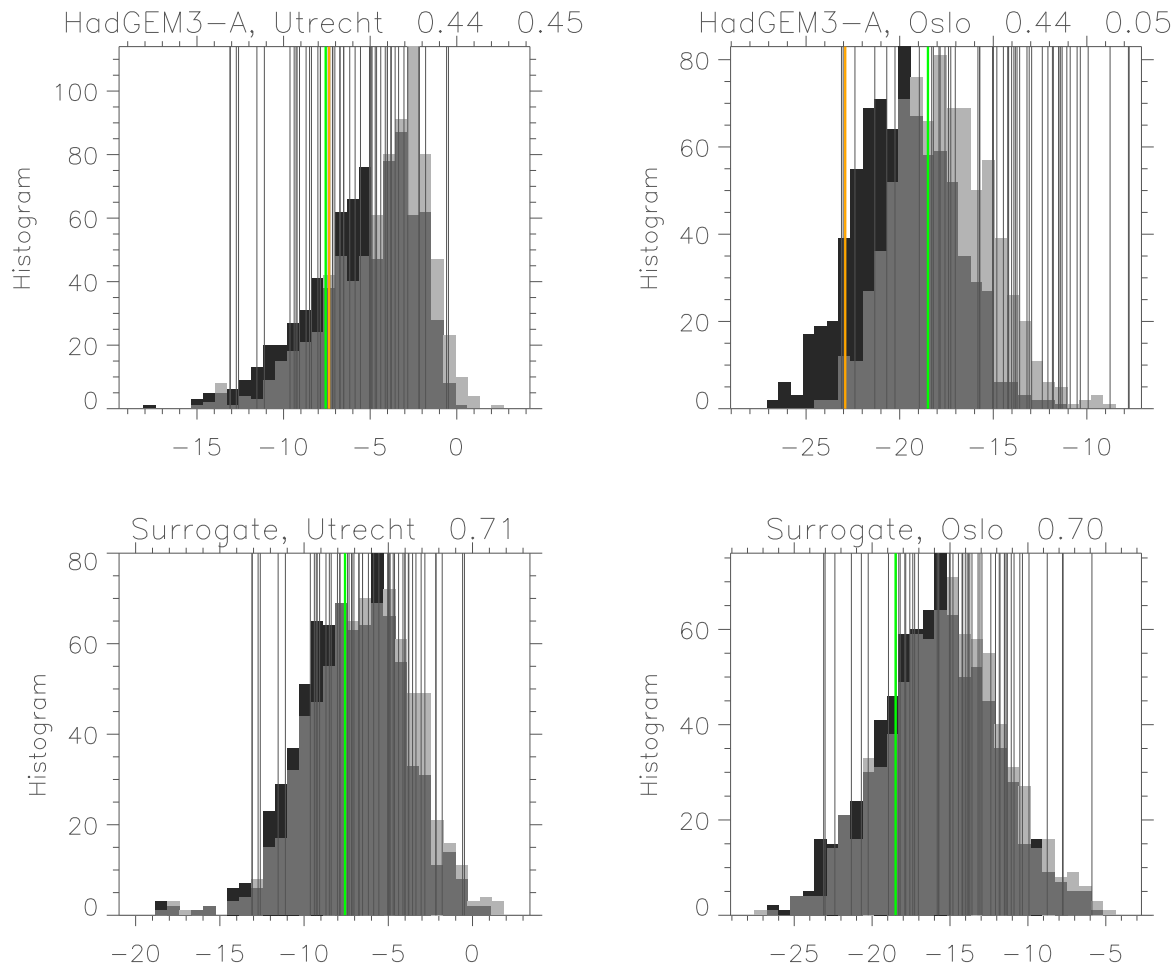


FIG. 11. As Fig. 9 but for the 5 % quantile of winter anomalies of grid-point temperatures [$^{\circ}\text{C}$].

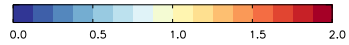
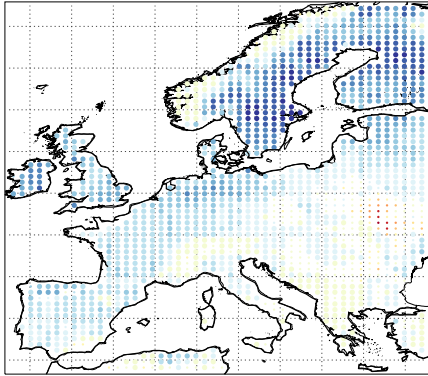


869 FIG. 12. Time development for spatial mean of temperature [$^{\circ}\text{C}$], standard deviation [$^{\circ}\text{C}$], and skewness.
 870 Standard deviation and skewness calculated from anomalies. Observations (green), HadGEM3-A historical
 871 (orange), surrogate perturbed (cyan).

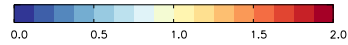
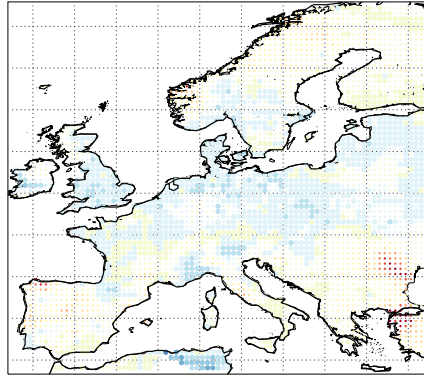


872 FIG. 13. The distributions of the temperatures [$^{\circ}\text{C}$] of the coldest day in winter for grid-points near Utrecht
 873 and Oslo. Based on 15*53 winters. Historical or perturbed climate: light shading. Histnat or unperturbed
 874 climate: dark shading. Thin vertical gray lines are the observed winters. Green vertical line is the observed
 875 winter 2009-2010. Orange vertical line is this winter corrected with mean bias. Risk ratios are provided at the
 876 top of the panels. For the HadGEM3-A the second number includes bias correction.

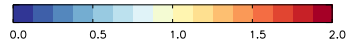
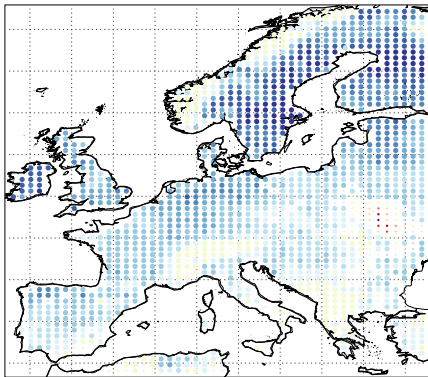
Risk ratio, HadGEM3-A



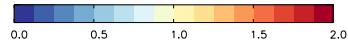
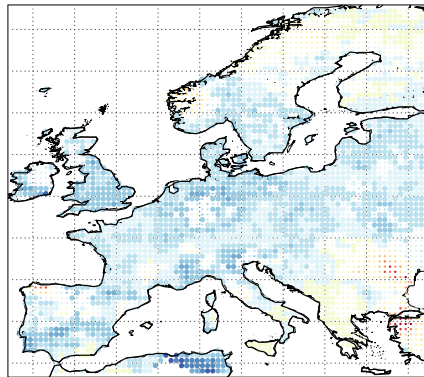
Risk ratio, Surrogate



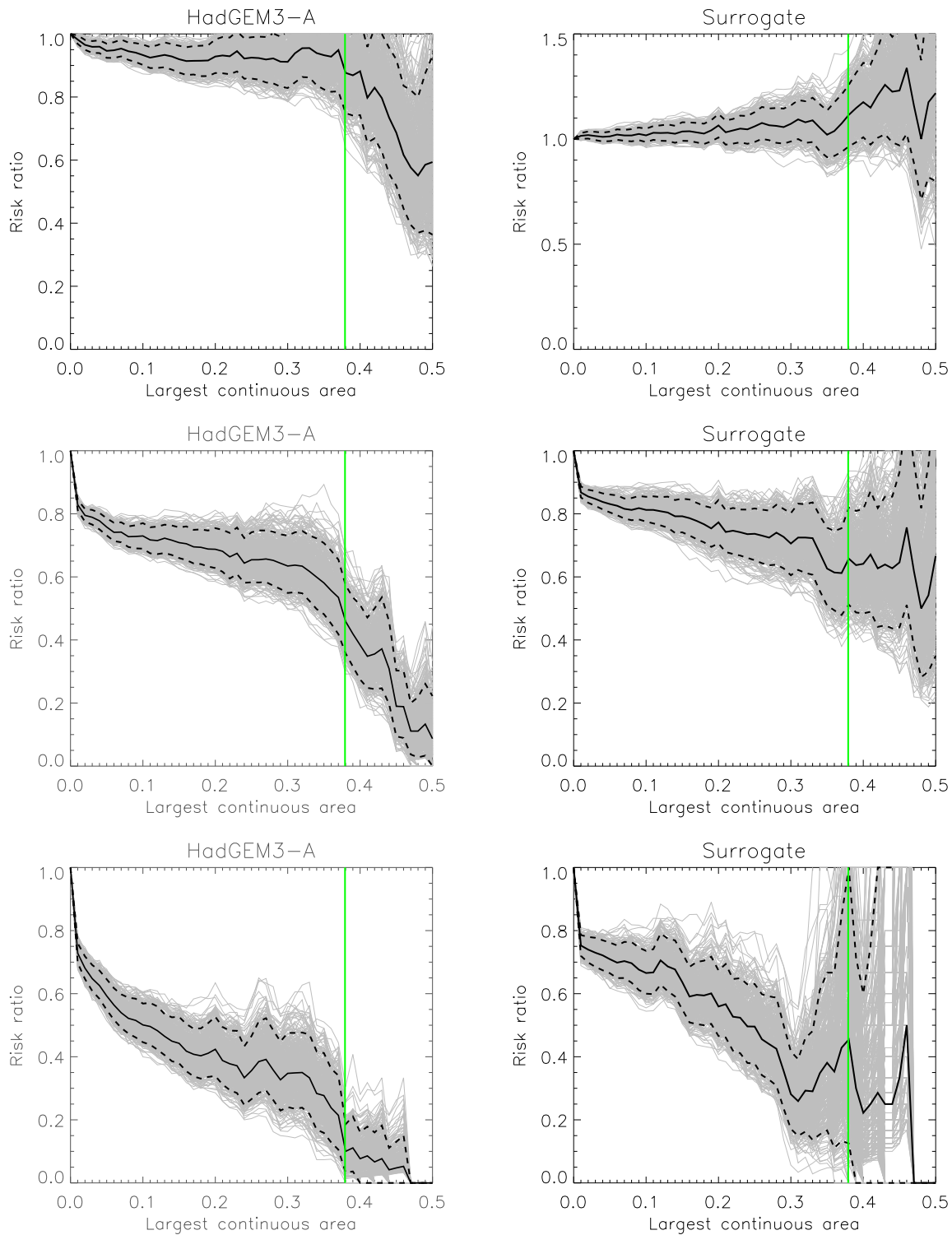
Risk ratio, HadGEM3-A



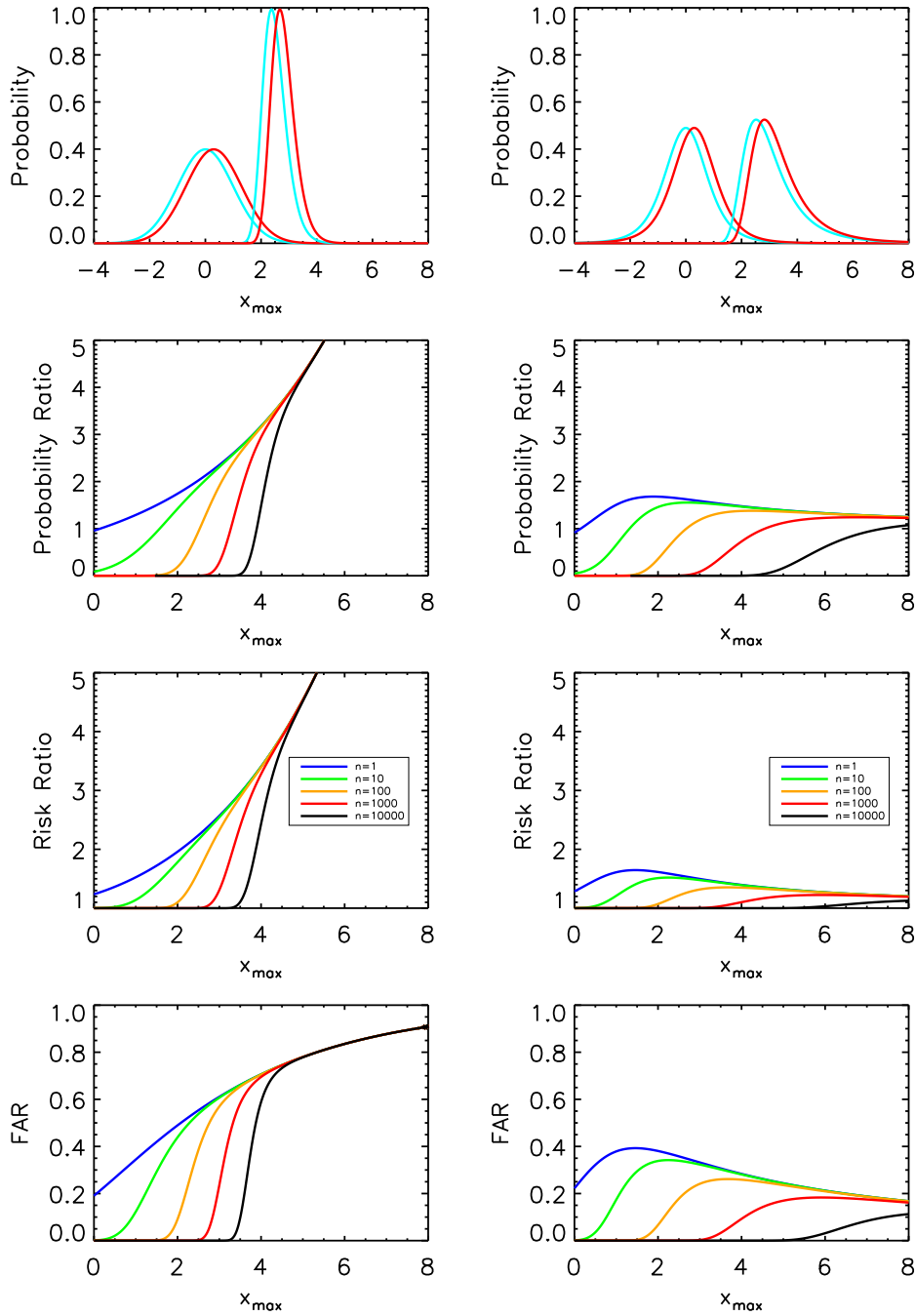
Risk ratio, Surrogate



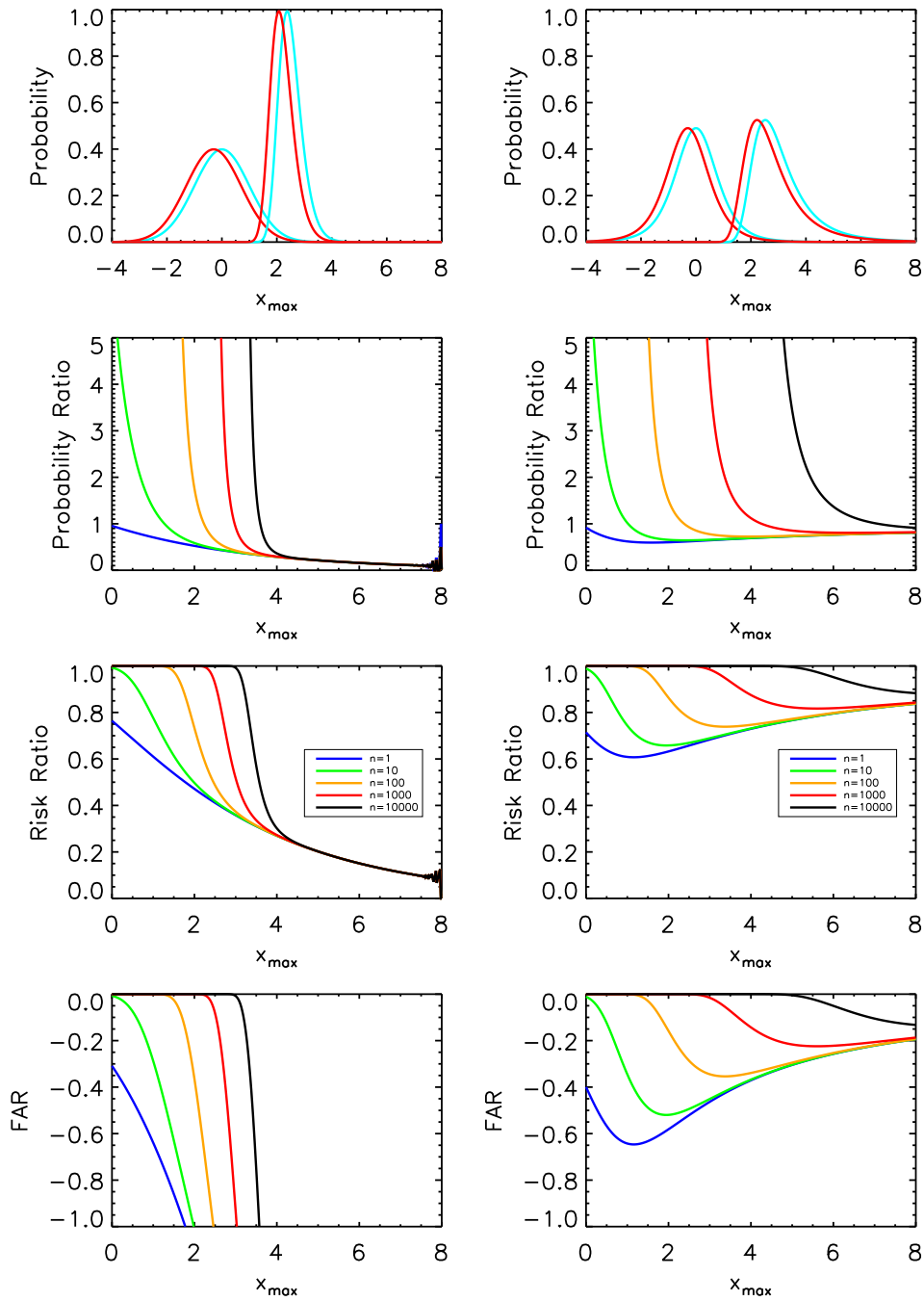
877 FIG. 14. Maps of the risk ratios of the temperature of the coldest day in the winter 2009-2010. Densities
878 calculated over all winter days. Left: HadGEM3-A. Right: Surrogate method. Top: based on the full period
879 1960-2013. Bottom: Based on 1985-2013. Large dots where the ratio is estimated to be significantly different
880 from 1 (5 % level).



881 FIG. 15. The risk ratio (thick black curve) for the blob index, i.e., the largest continuous area with temper-
 882 ature anomalies less than -2σ . Vertical green line: observed value for winter 2009-2010. Thin black curves:
 883 bootstraps. Black dashed curves: 95 % confidence interval. Left: HadGEM3-A. Right: Surrogate method. Top:
 884 based on the full period 1960-2013. Middle: Based on 1985-2013. Bottom: Based on 2007-2012.



885 Fig. A1. First row: Probability densities of the largest value, x_{max} , of n independent and identically distributed
 886 variables for $n = 1$ and $n = 100$. Cyan: the unperturbed case, p_1^{uc} and p_{100}^{uc} . Red: under climate change, p_1^{pc} and
 887 p_{100}^{pc} . The perturbed and unperturbed cases related by $p_1^{pc}(x) = p_1^{uc}(x - c)$, $c = 0.3$. These curves are shown in
 888 logarithmic scale in Fig. S4 in the supplement. Second, third and fourth rows: The ratio of probabilities p_n^{pc} / p_n^{uc} ,
 889 the risk ratios $RR = (1 - P_n^{pc}) / (1 - P_n^{uc})$, and the FARs $\frac{(1 - P_n^{pc}) - (1 - P_n^{uc})}{(1 - P_n^{pc})} = 1 - 1/RR$ as function of x_{max} . In left
 890 panel p_1^{uc} is Gaussian, in right panel it is t-distributed with 5 degrees of freedom. In each panel are shown results
 891 for $n=1$ (blue), 10 (green), 100 (orange), 1000 (red), 10000 (black).



892 Fig. A2. As for Fig. A1 but with the perturbed climate given by $p_1^{pc}(x) = p_1^{uc}(x+c)$, $c = 0.3$, indicating
 893 fewer positive extremes in the perturbed climate.